Colonic healing requires WNT produced by epithelium as well as Tagln^{+} and Acta2^{+} stromal cells

Soumyashree Das[1,#], Qiang Feng[1,#], Iyshwarya Balasubramanian[1,#], Xiang Lin[2], Haoran Liu[2], Oscar Pellón-Cardenas[3], Shiyan Yu[1], Xiao Zhang[1], Yue Liu[1], Zhi Wei[2], Edward M. Bonder[1], Michael P. Verzi[3, 5], Wei Hsu[4], Lanjing Zhang[5, 6], Timothy C. Wang[7], Nan Gao[1, 5]*

1. Department of Biological Sciences, Rutgers University, Newark, New Jersey, USA
2. Department of Computer Science, New Jersey Institute of Technology, New Jersey, USA
3. Department of Genetics, Rutgers University, Piscataway, New Jersey, USA.
4. Department of Biomedical Genetics, Center for Oral Biology, James P Wilmot Cancer Center, University of Rochester Medical Center, Rochester, New York, USA
5. Rutgers Cancer Institute of New Jersey, New Brunswick, NJ 08901, USA
6. Department of Pathology, University Medical Center of Princeton, Plainsboro, New Jersey, USA.
7. Department of Medicine, Division of Digestive and Liver Diseases, Irving Cancer Research Center, Columbia University, New York, New York, USA.

Key words: Wntless, Wnt, Tagln, Acta2, Gpr177, Colitis, Wound Healing, Intestinal Stem Cell.

***Correspondence to:** Nan Gao, Ph.D., Department of Biological Sciences, Rutgers University, Newark, NJ 07102, USA.
Email: ngao@rutgers.edu

# These authors contributed equally to this study.

The authors have no conflict of interest to declare.

ABSTRACT

While Wnt signaling is clearly important for the intestinal epithelial homeostasis, the relevance of various sources of Wnt ligands themselves remains incompletely understood. Wnt blockage in distinct stromal cell types suggested obligatory functions of several stromal cell sources and yielded different observations. The physiological contribution of epithelial Wnt to tissue homeostasis remains unclear. We show here that blocking epithelial Wnts affected colonic $Reg4^{+}$ epithelial cell differentiation, and impaired colonic epithelial regeneration after injury. Single cell RNA analysis of intestinal stroma showed that the majority of Wnt-producing cells were contained in transgelin (Tagln+) and smooth muscle actin alpha 2 (Acta2+) expressing populations. We genetically attenuated Wnt production from these stromal cells using Tagln-Cre and Acta2-CreER drivers, and found that Wnt blockage from either epithelium or Tagln+ and Acta2+ stromal cells impaired colonic epithelial healing after chemical-induced injury. Aggregated Wnt blockage from both epithelium and Tagln+ or Acta2+ stromal cells drastically diminished epithelial repair, increasing morbidity and mortality. These results from two uncharacterized stromal populations suggested that colonic recovery from colitis-like injury depends on multiple Wnt-producing sources.

INTRODUCTION

Wingless-type MMTV integration site family members (Wnts) are secreted glycolipoproteins engaging in short-range signaling (Willert et al., 2003; Willert and Nusse, 2012). Newly synthesized Wnt proteins are lipidated in endoplasmic reticulum by an acyltransferase Porcupine (Porcn)(Takada et al., 2006) then transported by Wntless (Wls, or Gpr177 in mice) transmembrane protein for secretion (Banziger et al., 2006; Bartscherer et al., 2006). Binding of extracellular Wnts to their Frizzled receptors in ligand-receiving cells initiate a signal cascade (Schulte, 2010; Schulte and Bryja, 2007; Wu and Nusse, 2002), inactivating the glycogen synthase kinase 3 (GSK3)-containing cytoplasmic destruction machinery and stabilizing β-Catenin (Cadigan and Peifer, 2009; Huang and He, 2008; MacDonald et al., 2009). Binding of β-Catenin to Tcf factors in nucleus drives a gene program related to cellular growth and proliferation (He et al., 2004; MacDonald and He, 2012; Tamai et al., 2000; Wehrli et al., 2000). Abnormal activation of canonical Wnt pathway in most human colon cancers highlights

its profound influence on cellular behavior (Angers and Moon, 2009; Clevers and Nusse, 2012; de Lau et al., 2007; MacDonald et al., 2009; Nusse et al., 2008; Polakis, 2007; Reya and Clevers, 2005). Noncanonical Wnt molecules also activate pathways such as Rho family small GTPases to control cellular migration (Boutros and Mlodzik, 1999; Eaton et al., 1996; Fanto et al., 2000; Habas et al., 2003; Habas et al., 2001; Sakamori et al., 2014; Strutt et al., 1997; Wallingford and Habas, 2005).

The development and maintenance of intestinal epithelium depend on intact Wnt signaling. Removing β-Catenin or Tcf4 from mouse intestinal epithelia impaired crypt formation causing lethality (Fevr et al., 2007; Korinek et al., 1998; van de Wetering et al., 2002; van Es et al., 2012). Systemic overexpression of a Wnt antagonist Dickkopf homolog 1 induced severe damages to adult intestines (Kuhnert et al., 2004; Pinto et al., 2003). While Wnt signaling is clearly important, the importance of Wnts themselves is not as clear. Paneth cells were first shown as the primary source of Wnts in small intestine (Gregorieff et al., 2005); *ex vivo* cultured $Lgr5^+$ intestinal stem cell (ISC) (Barker et al., 2007), when associated with Paneth cells, showed enhanced enteroid-forming capability (Sato et al., 2011). Enteroids lacking *Wnt3* could not be properly passaged (Farin et al., 2012), while enteroids lacking *Wls* or *Porcn* failed to grow *ex vivo* (Kabiri et al., 2014; Valenta et al., 2016). The growth of above epithelial Wnt deficient enteroids could nevertheless be rescued via supplementing stromal cells or stromal Wnt proteins to the culture (Kabiri et al., 2014; Valenta et al., 2016) (Farin et al., 2012). These observations, combined with the overall lack of *in vivo* phenotype in the absence of epithelial *Wnt3* (Farin et al., 2012), *Vps35* (de Groot et al., 2013), *Porcn* (Kabiri et al., 2014; San Roman et al., 2014), or *Wls* (Valenta et al., 2016) collectively suggested that while epithelial Wnts were required to support ISCs *ex vivo*, their physiological relevance remained unclear in the presence of a potentially redundant stromal source of Wnt. The question regarding the importance of Wnts themselves was further highlighted by the observation that R-spondin was more powerful than Wnts in activating Wnt signaling (Yan et al., 2017).

Existing literature suggested a complexity and functional divergence of various stromal sources of Wnt. The stroma of the intestinal lamina propria consist myofibroblasts, fibroblasts, vascular and visceral smooth muscles, as well as innate and professional immune cells (Powell et al., 2011). Some of these cell lineages express Wnt2b, Wnt4, and Wnt5a (Farin et al., 2012; Gregorieff et al., 2005; Miyoshi et al., 2012). *Myh11-CreER* mediated ablation of

Porcn in intestinal myofibroblasts alone, or in combination with epithelial *Porcn* deletion, did not perturb intestinal epithelial homeostasis (San Roman et al., 2014), marking myofibroblasts a non-essential stromal Wnt source. However, deleting *Porcn* from myofibroblasts expressing Pdgf receptor alpha (Pdgfrα) blocked intestinal crypt formation (Greicius et al., 2018). Foxl1-expressing cells were subsequently identified as Pdgfrα+ telocytes immediately juxtaposing epithelium, produced Wnts, R-spondin 3, and Gremlin proteins, while lacked myofibroblast markers. Genetic ablation of Foxl1+ cells, or blockage of Wnt production from Foxl1-expressing cells, disrupted ISC homeostasis in both small intestine and colon (Aoki et al., 2016; Shoshkes-Carmel et al., 2018). McCarthy and coworkers recently identified a Gremlin1-producing $CD81^{+}$ $Pdgfra^{low}$ population, referred to as trophocytes, present just below crypts and contribute to ISC maintenance in vivo (McCarthy et al., 2020). In the colon, CD34+; α-smooth muscle actin negative pericryptal stromal cells expressing Wnt2b, R-spondin 1, and Gremlin 1, were shown to support Lgr5+ ISCs *ex vivo* (Stzepourginski et al., 2016). Blocking Wnt secretion from a heterogenous Gli1+ stromal population disrupted colonic crypt homeostasis (Degirmenci et al., 2018). In small intestines, however, these Wnt2b-enriched Gli1+ cells were proposed to be a reserve Wnt source for epithelial Wnt deprivation. In addition to above homeostasis conditions, $Wnt5a^{+}$ mesenchymal cells were also shown to promote colonic crypt regeneration after biopsy injury (Miyoshi et al., 2012), whereas Wnt deprivation from intestinal mononuclear phagocytes exacerbated irradiation-induced mucosal damage (Saha et al., 2016).

Above studies, on the one hand, illustrated ISC-supporting roles of Wnt-producing epithelial and stromal cell types, but on the other hand led to perplexing questions. First, if Wnts from certain stromal cell type are obligatory for ISC homeostasis in vivo, then what is the physiological purpose of making epithelial Wnts, especially those from Paneth cells having the prime access to ISCs in the small intestine. Second, transcriptomes of Gli1+ or Pdgfrα+ cells appeared to intersect those of myofibroblasts, yet different Cre drivers yielded distinct, sometimes opposite, outcomes regarding to whether, when, and where an intestinal phenotype was observed (Degirmenci et al., 2018; San Roman et al., 2014) (Greicius et al., 2018; Shoshkes-Carmel et al., 2018). It is also plausible that: (i) instead of the existence of a specific obligatory Wnt-supplying cell type, the quantity of Wnt molecules collected from various adjacent sources in the niche may be critical for intestinal homeostasis; and (ii) epithelial Wnt

production may be essential during mucosal injury that disrupts epithelial-mesenchymal interactions. Based on these hypotheses, we describe the under-appreciated role of epithelial Wnts in homeostasis and during various injuries. A single cell (sc) RNA survey of intestinal stroma revealed that mesenchymal Wnt producers were constrained to cell clusters expressing *Transgelin* (Tagln, also known as SM22α) (Dong et al., 2012) or *Acta2*. By using Tagln-Cre and Acta2-CreER drivers to abrogate Wnt productions in these stromal subsets, we demonstrate that the abundance of Wnts collected from multiple tissue sources at the regenerating niche may be critical for colonic healing after injury.

RESULTS

Blocking epithelial Wnts impaired colonic Reg4 cell differentiation

Global or tissue specific ablation of Wls (Gpr177 in mouse) in various animals caused phenotypes resembling loss of Wnt signaling (Banziger et al., 2006; Bartscherer et al., 2006; Fu et al., 2009) due to its indispensable function for Wnt secretion (Ching and Nusse, 2006; Das et al., 2012; Port and Basler, 2010). Using constitutive (*Villin-Cre*) or inducible (*Villin-CreER*) intestinal epithelial cell (IEC) drivers, we performed *Gpr177* ablation to abrogate epithelial Wnt production. Mice lacking IEC-specific *Gpr177* did not show histological abnormality in small intestines **(Fig. 1A)** or alterations in Paneth or mitotic cell numbers in the crypts **(Fig. 1B, C**, quantified from 3 mice for each genotype**)**. The deletion of *Gpr177* specifically in IECs was further assessed by immune-gold labeling of endogenous Gpr177 in wild type (WT) and *Gpr177$^{L/-}$; Vil-Cre* intestines. Gpr177^{+} gold particles were diminished by 90% in endoplasmic reticulum (ER), 91% in non-ER cytoplasmic region, and 93% in plasma membrane of *Gpr177*-deficient Paneth cells **(Suppl. Fig. 1A, B, quantified in Suppl. Fig. 1C)**. No obvious change was detected in stromal cells of the same tissues **(Suppl. Fig. 1A, B)**.

Despite the lack of histological abnormality, *Gpr177*-deficient colonic epithelium had a significant reduction of Reg4+ cells, previously reported as deep crypt secretory (DCS) cells, in both *Vil-Cre* and *Vil-CreER* driven homozygotes **(Fig. 1D, E)**. This change has not been previously reported and was specific to Reg4+ cells. No change was found in the number of Muc2+ goblet cells in the same tissues **(Fig. 1D, E, Suppl. Fig. 1D)**. The number of nuclear β-catenin^{+} cells in both small intestine and colonic epithelia were equivalent between wild type (WT) and *Gpr177*-deficient epithelium **(Fig. 1F, G, Suppl. Fig. 1E)**. Quantitative RT-PCR

supported the immunohistochemistry finding that there was no transcriptional alteration in canonical Wnt targets as well as Paneth cell genes **(Suppl. Fig. 1F)**.

Gpr177$^{L/L}$;Vil-Cre mouse crypts failed to develop into enteroids in regular ENR medium *ex vivo* **(Suppl. Fig. 1G)**. The enteroid growth could be partially restored if recombinant Wnt3a or CHIR (the GSK3 inhibitor) was supplemented at seeding **(Suppl. Fig. 1G).** We then cultured enteroids from non-induced adult *Gpr177$^{L/-}$;Villin-CreER* mice in ENR medium for 4 days, followed by 4-OHT administration for 12 hrs to induce *Gpr177* deletion. Addition of 4-OHT, but not vehicle, caused growth arrest of nearly 90% *Gpr177$^{L/-}$;Vil-CreER* enteroids 5 days after 4-OHT treatment **(Fig. 1H, I)**. Recombinant Wnt3a proteins, when added into ENR medium upon 4-OHT withdrawal, significantly improved the survival and growth of *Gpr177$^{L/-}$;Vil-CreER* enteroids, judged by enteroid budding morphologies and EdU incorporation **(Fig. 1H, I)**. These results documented a previously undescribed blockage of Reg4 cell differentiation in colon upon epithelial Wnt blockage.

Tagln+ stromal domain encompasses subepithelial Wnt producers

Previous studies investigating sources of stromal Wnts utilizing Myh11, Gli1, Pdgfrα, Cd81 or Foxl1 as markers suggested partial overlap among these cell populations, but the extent was not examined in detail. To gain a systematic understanding of the overall distribution of Wnt-producers within intestinal stroma, we conducted a single-cell RNA sequencing (scRNA-Seq) analysis of mouse total ileal stromal tissue. Uniform manifold approximation and projection (UMAP) analyses revealed 22 cell clusters encompassing major lamina propria cell types **(Fig. 2A)**. By examining all mouse Wnt genes, we were able to map 6 major Wnt-expressing cell clusters **(Fig. 2A)**. Cluster 9 was identified as the largest Wnt4- and Wnt5a-expressing cluster co-expressing *Foxl1, Pdgfrα,* and *Gli1* **(Fig. 2B)**. This cluster also robustly expressed *Tagln, Acta2*, and *Myh11*, genes expressed by fibroblast, myofibroblast, and smooth muscle cells. Other Wnt4- and Wnt5a-expressing clusters are 5, 11, 14, and 21, where small number of Foxl1+ cells were found. Clusters 5, 11, and 21 co-expressed high levels of *Pdgfrα* while cluster 14 did not. Gli was highly expressed in 5 and 14 while not so in clusters 11 and 21. However, all these clusters were marked by *Tagln* and *Acta2* **(Fig. 2B)**. In contrast to the Wnt4- and Wnt5a- expressing clusters, cluster 15 was defined by Wnt2b-expressing *Pdgfra*^{low} trophocytes as observed by the presence of *Cd81* and *Grem1* (McCarthy et al.,

2020), and the absence of *Foxl1*. In addition, this cluster expressed lower abundance of *Tagln*, *Acta2*, and *Myh11* **(Fig. 2B)**. Examination of *Tagln*-expressing, Wnt-producing clusters 5, 9, 11, 14, and 21, in light of *Pdgfra*, *Gli1*, and *Foxl1* suggested that they were substantially overlapped by *Tagln*, *Acta2*, and *Myh11*-expressing cell populations **(Fig. 2C)**.

Compared to the population that do not express *Wnt2b*, *Wnt4*, or *Wnt5a*, cells expressing high abundance of these ligands also expressed abundant *Tagln* and *Acta2* compared to *Gli1* and *Foxl1* **(Fig. 2D)**. We then used a Single Cell Deep Constrained Clustering (scDCC) approach, a newly developed deep learning model that guides the clustering by giving weight to marker genes (here we used Wnt5a and Wnt4, respectively). These Wnt-based clustering demonstrated a high abundance of *Tagln*, *Acta2*, *Pdgfra*, *Myh11*, *Gli1*, *Foxl1* and a low abundance of *Cd81* in *Wnt5a*-expressing and Wnt4-expressing stromal clusters (circled) **(Suppl. Fig. 2A and 2B)**.

Compared to the heterogeneous nature of *Gli1*+ cells (Degirmenci et al., 2018), *Foxl1*$^{+}$ telocytes represented a specific cell population shown to support ISC homeostasis (Shoshkes-Carmel et al., 2018). The majority of *Foxl1*-expressing cells also expressed *Tagln* **(Fig. 2E)**, and *Tagln* was not detected in 16 *Foxl1*+ cells. Examining the transcriptome of *Foxl1+/Tagln-* and *Foxl1+/Tagln+* cells revealed their high expression of *Wnt4*, *Wnt5a*, *Pdgfra*, and *Gli1* **(Fig. 2F)**. Gene specific analysis (GSA) identified only 6 genes differentially expressed between *Foxl1+/Tagln-* and *Foxl1+/Tagln+* populations while 614 genes were differentially expressed between *Foxl1-/Tagln+* and *Foxl1+/Tagln+* populations **(Suppl. Fig. 2C-G)**, suggesting that Foxl1 defines a strict subset of *Tagln+* cell population. Overall, these analyses revealed that *Tagln+* domains encompassed the major stromal Wnt producers, and there was a high degree of overlap among reported stromal cell lineages, except for *Pdgfra*^{low} trophocytes (McCarthy et al., 2020).

Tagln-Cre and Acta2-CreER targeted intestinal stromal domains

Examination of endogenous Tagln expression revealed a mesenchymal domain throughout the intestinal tract **(Fig. 3A)**, consistent with its reported expression in fibroblasts, myofibroblasts, and smooth muscles (Katajisto et al., 2008; Kuhbandner et al., 2000) (Dong et al., 2012). In duodenum and ileum, we found that subset of Tagln-expressing cells was in

immediate proximity of crypt cells, wrapping the epithelial glands and extending into villus mesenchymal region **(Fig. 3A)**. Similar pattern was found in colon **(Fig. 3B)**.

We crossed *Tagln-Cre* mouse (Boucher et al., 2003; Holtwick et al., 2002) to *Rosa26R* reporter mice (Srinivas et al., 2001), and found that *Tagln-Cre* activated reporter expression in a pattern similar to endogenous *Tagln* **(Fig. 3C**, please compare to 3A**)**. We next stained for endogenous Wnt proteins in *Tagln-Cre;Rosa26R*^{EYFP} mouse intestinal tissues. In both small intestine and colon, a subset of Tagln-Cre expressing cells (EYFP+) co-expressed Wnt2b **(**white arrows, **Fig. 3D, E**). Some Wnt2b-expressing Tagln+ cells showed large cell body with long processes and located underneath the epithelium **(Fig. 3D)**, resembling what was described for telocytes. Close examination revealed Wnt2b+ vesicular puncta in vicinity of cells with strong cytoplasmic Wnt2b staining (arrowheads in **Fig. 3E, Suppl. Fig. 3A)**. Subset of Tagln-Cre expressing cells expressed endogenous Wnt5 **(Fig. 3F, G)**, and tended to show a different localization and cell shapes. Close examination revealed both perinuclear and vesicular localization of Wnt5 **(Suppl. Fig. 3B)**. Examination of GFP positivity for Wnt2b+ or Wnt5+ cells suggested that the majority of them were labeled by Tagln-Cre **(Fig. 3H)**, consistent with scRNA-Seq results **(Fig. 2C, D)**.

In addition to *Tagln-Cre*, we also examined the *Acta2-CreER* driver (a knockin allele referred to as *Acta2-CreER* hereafter) (Manieri et al., 2015), and observed a slightly narrow Cre-expressing stromal domain, with scattered EYFP+ cells detected in the lamina propria of villi in *Acta2-CreER*;*Rosa26R*^{EYFP} mice **(Fig. 3I)**. The relatively constrained Acta2-CreER activity reflected a potential mosaic recombination by this tamoxifen-inducible line, as opposed to the constitutive expression of Tagln-Cre. We then used these two stromal drivers to assess the contribution of Wnts produced by Tagln+ and Acta2+ cells to intestinal homeostasis, which have not been studied before.

Blocking Wnt production from epithelium and Tagln+ or Acta2+ cells diminished colonic Reg4 cells

We crossed Gpr177 flox mice to *Tagln-Cre* and *Acta2-CreER* mice, respectively. *Gpr177*$^{L/L}$*; Tagln-Cre* mice did not display global intestinal defects. Similarly, tamoxifen treated *Gpr177*$^{L/L}$*; Acta2-CreER* mice did not exhibit any defects, observations reminiscent of a previous report using *Myh11-Cre* to delete *Porcn* in myofibroblasts (San Roman et al., 2014). We then

developed *Gpr177$^{L/-}$;Vil-Cre;Tagln-Cre* as well as *Gpr177$^{L/-}$;Vil-Cre;Acta2-CreER* mice to remove Gpr177 from both epithelium and Tagln+ or Acta2+ stromal cells. In situ hybridization for *Gpr177* showed effective gene ablation in both epithelial and stromal compartments **(Suppl. Fig. 4A, B)**.

Gpr177$^{L/-}$;Vil-Cre;Tagln-Cre mouse intestines appeared histologically normal **(Fig. 4A)** but with reduced crypt base columnar cells (CBC) marked by *Olfm4* by in situ (**Fig. 4C**, quantified in **4B**), Paneth cells (**Fig. 4D**, quantified in **4B**), and proliferative cells marked by 30 min EdU labeling (**Fig. 4E**, quantified in **4B**) or by PCNA staining **(Suppl. Fig. 4C)**. No change was detected for nuclear β-catenin^{+} cells **(Fig. 4F**, quantified in **4B)**. Examination of *Gpr177$^{L/-}$;Vil-Cre;Tagln-Cre* mouse colons showed a notable alteration of glandular morphology **(Fig. 4G)**, accompanied by a diminished number of Reg4^{+} cells (**Fig. 4H**, quantified in **4I**). Goblet cells remained unchanged in the same tissue **(Fig. 4H,** quantified in **4I**, also see **Suppl. Fig. 4D)**.

A similar reduction of colonic Reg4^{+} cells was observed in *Gpr177$^{L/-}$;Vil-Cre;Acta2-CreER* mice **(Fig. 4H)**, but to a less extent compared to *Gpr177$^{L/-}$;Vil-Cre;Tagln-Cre* mice **(Fig. 4I)**. However, *Gpr177$^{L/-}$;Vil-Cre;Acta2-CreER* mice did not show other changes in CBC, Paneth cells or proliferative cells **(Fig. 4A-F)**. Quantitative RT-PCR analysis showed a significant reduction in *Gpr177* transcripts in *Gpr177$^{L/-}$;Vil-Cre;Acta2-CreER* intestine **(Suppl. Fig. 4E)**, suggesting the lack of phenotypic difference was not due to an inefficient deletion.

Quantitative RT-PCR analysis detected a significantly reduced *Mmp7* in *Gpr177$^{L/-}$;Vil-Cre;Tagln-Cre* intestines **(Fig. 4J)**, and reduced *Defa5* in *Gpr177$^{L/-}$;Vil-Cre;Acta2-CreER* intestines **(Fig. 4K)**. *Mmp7* and *Defa5* represented signature markers of mature Paneth cells. These results suggested an additive impact of Wnts from epithelium and Tagln+ or Acta2+ stromal cells on Reg4+ cell differentiation.

Blocking Wnts from epithelium and Tagln+ cells modestly affected regeneration following irradiation

Whole body irradiation rapidly eliminates proliferating intestinal stem cells (ISCs) (Potten, 1977) and elicits epithelial regeneration (Yu et al., 2018b; Zhang et al., 2020). We asked whether Wnts produced in epithelium and Tagln stromal cells participated in irradiation-induced regeneration. Adult *control*, *Gpr177$^{L/L}$;Vil-Cre*, and *Gpr177$^{L/L}$;Vil-Cre;Tagln-Cre* mice (all littermates) received 12 Gy whole body irradiation (n=6 for each genotype, from at least 3

different litters). All mice showed a similar trend of body weight loss starting from day 3 **(Fig. 5A)**. On day 5, wild type and *Gpr177$^{L/L}$; Vil-Cre* mice showed a weight gain while *Gpr177$^{L/L}$;Vil-Cre;Tagln-Cre* mice displayed the smallest weight gain ($p<0.05$, **Fig. 5A**). Upon sacrifice, *Gpr177$^{L/L}$;Vil-Cre;Tagln-Cre* intestines showed reduced number of regenerative crypts **(Fig. 5B**, quantified in **5D)**, proliferative cells **(Fig. 5C-D)**, CBC and Paneth cells **(Fig. 5D-E)**. *Gpr177$^{L/L}$;Vil-Cre* mice only exhibited a moderate reduction of Paneth cells ($p<0.05$, **Fig. 5D-E**). Nuclear β-Catenin^{+} cells were significantly reduced in crypts of regenerating *Gpr177$^{L/L}$;Vil-Cre;Tagln-Cre* intestines (two morphologically different regions shown in **Fig. 5F-G**). The observed modest reduction of body weight and epithelial regeneration in *Gpr177$^{L/L}$;Vil-Cre;Tagln-Cre* mice collectively indicated a resilience to abrogated Wnt production from the epithelium and Tagln+ stromal cells under the context of irradiation.

Colonic healing from DSS-induced mucosal injury requires Wnts from epithelial and Tagln+ and Acta2+ stromal cells

Compared to irradiation that primarily eliminated cycling ISCs, dextran sulfate sodium (DSS) induces mucosal demolishing damage, characterized by epithelial death, ulceration, impairment of glandular architecture, and inflammation. Upon DSS withdrawal, colonic epithelia heal through regeneration (Yu et al., 2020). As Wnt signaling was shown to play a role in DSS-induced epithelial recovery (Koch et al., 2011), we further asked whether colonic epithelial restoration required Wnts from epithelial or Tagln+ and Acta2+ cells. We treated *Gpr177$^{L/L}$;Vil-Cre* (n=10), *Gpr177$^{L/L}$;Vil-Cre;Tagln-Cre* mice (n=6) with 2.5% DSS in drinking water for 7 days and returned them to regular water for another 7 days to allow recovery **(Fig. 6A)**. We used littermates that were Cre negative, as well as mice expressing Cre only, and tamoxifen-injected WT and Vil-CreER mice (non-littermates) as controls (n=13). Strikingly, compared to control mice, *Gpr177$^{L/L}$;Vil-Cre* and *Gpr177$^{L/L}$;Vil-Cre;Tagln-Cre* mice showed significantly more body weight losses **(Fig. 6B)**. All control mice and most *Gpr177$^{L/L}$;Vil-Cre* mice survived the entire 14-day procedure, whereas *Gpr177$^{L/L}$;Vil-Cre;Tagln-Cre* mice exhibited mortality from day 9 **(Fig. 6C)**, an early point of recovery. *Gpr177$^{L/L}$;Vil-Cre;Tagln-Cre* survivors did not exhibit body weight gain, which was observed for wild type and *Gpr177$^{L/L}$;Vil-Cre* mice during recovery phase **(Fig. 6B).** *Gpr177$^{L/L}$;Vil-Cre;Tagln-Cre* survivors showed shortened colons upon sacrifice on day 14 **(Fig. 6A)**.

Pathological evaluation revealed greater epithelial damages in *Gpr177$^{L/L}$;Vil-Cre* mice than wild type, and the worst colitis in *Gpr177$^{L/L}$;Vil-Cre;Tagln-Cre* mice on day 14 **(Fig. 6D, E).** Colitis scoring based on ulceration, crypt death, immune cell infiltration, thickness of colonic wall, and loss of goblet cell, reached the same conclusion for day 11 **(Suppl. Fig. 5B)**.

Control mouse colonic mucosa collected on day 11 already exhibited prominent wound healing activities including the formation of nascent crypts flanking the wound, epithelial proliferation and migration towards the surfaces of the wound (red brackets designate ulceration, **Fig. 6D**). Control mouse mucosa showed near complete healing on day 14 exemplified as a restoration of goblet cell-filled glandular structures **(Fig. 6F)**. In contrast, *Gpr177$^{L/L}$;Vil-Cre* and *Gpr177$^{L/L}$;Vil-Cre;Tagln-Cre* mice had significantly larger and more ulcerations at the beginning and end of recovery **(Fig. 6D, G)**. On day 11, *Gpr177$^{L/L}$;Vil-Cre;Tagln-Cre* mouse colons showed continuous ulceration, massive immune cell infiltration, and a severely thickened colonic wall **(Fig. 6D)**. On day 14, *Gpr177$^{L/L}$;Vil-Cre;Tagln-Cre* survivors had scattered colonic crypts with diminished goblet cell differentiation **(Fig. 6D, F)**.

The impact of Gpr177 removal from intestinal epithelium or Tagln+ stromal cells on colonic epithelial resolution demonstrated here was never described. We therefore also performed DSS experiments on *Gpr177$^{L/L}$;Vil-CreER* mice to validate this finding. Tamoxifen-induced *Gpr177$^{L/L}$;Vil-CreER* mice showed a similarly exacerbated colitis morbidity as seen for *Gpr177$^{L/L}$;Vil-Cre* mice **(Fig. 6B, H, I)**. Above changes were not due to toxicity of Cre or CreER, as mice expressing Cre or CreER only did not exhibit difference from wild type mice **(Suppl. Fig. 5A)**. In addition, we used a single administration of tamoxifen (75 mg/kg) in all our CreER experiments, and this was well below the reported toxicity-inducing dosage (Bohin et al., 2018; Huh et al., 2010). Indeed, wild type mice or CreER mice treated with this tamoxifen dosage did not show difference in terms of body weight recovery in response to DSS treatment **(Suppl. Fig. 5A)**.

As Acta2-CreER targeted a relatively restricted stromal domain **(Fig. 3I)**, we asked whether Wnts produced by Acta2+ stromal cells also contributed to colonic wound healing. Surprisingly, both *Gpr177$^{L/L}$;Acta2-CreER* (n=6) and *Gpr177$^{L/L}$;Vil-Cre;Acta2-CreER* (n=6) mice showed increased morbidity **(Fig. 6B, C).** We noted that *Gpr177$^{L/L}$;Vil-Cre;Acta2-CreER* mice showed a worse body weight recovery than *Gpr177$^{L/L}$;Acta2-CreER* mice starting from day 9 **(Fig. 6B)**. The slower recovery was consistent with their greater colitis shown at pathological level **(Fig.**

6H, I). These analyses suggested that Wnts produced by epithelial cells, Tagln+, and Acta2+ cells were all important for colonic wound healing and the disease severities were proportionally correlated with additive Wnt blockage from different tissue compartments.

Wnts from wound-associated Tagln+ cells are required for β-catenin nuclear localization in regenerative epithelium

DSS treatment disrupted the colonic mucosal microenvironment by severely demolishing glandular structure and epithelial-stromal interaction. We examined the localization of Tagln+ cells in DSS-treated colonic mucosa 4 days after withdrawing DSS treatment, a time point when epithelial recovery was prominent **(Fig. 7A)**. Compared to colons at steady states **(Fig. 3A)**, DSS-treated colons contained increased number of Tagln+ cells surrounding the hyperplastic crypts **(**white arrows, **Fig. 7B)**. Immediately flanking the ulcered region (asterisk in **Fig. 7A**), Tagln-expressing cells were detected at the base of nascent crypt **(**white arrows, **Fig. 7C)** and underneath the single layer of wound-covering epithelium **(**white arrows, **Fig. 7D).**

Within these regenerating epithelia associated with Tagln+ cells, epithelial cells with nuclear β-catenin were found **(**red arrows, **Fig. 7E-G)**. We found a significant reduction in such nuclear β-catenin+ regenerative epithelial cells in *Gpr177$^{L/L}$;Vil-Cre* **(Fig. 7H-J)** and *Gpr177$^{L/L}$;Vil-Cre;Tagln-Cre* colons **(Fig. 7K-M)**. Compared to *Gpr177$^{L/L}$;Vil-Cre* colons, *Gpr177$^{L/L}$;Vil-Cre;Tagln-Cre* colons showed a further reduction of nuclear β-catenin+ epithelial cells **(Fig. 7N)**. As Tagln+ cells were prominently observed near the injured epithelia **(Fig. 7O, P)**, these changes were apparently caused by lack of Wnt production in the niche rather than lack of Tagln+ cells. We further examined 3 canonical Wnt targets CD44, c-Myc, and Axin2 by immunostaining **(Suppl. Fig. 6A-C)**. *Gpr177$^{L/L}$;Vil-Cre;Tagln-Cre* colons showed the lowest CD44 and Axin2 in regenerative epithelia **(Suppl. Fig. 6B and C)**. These results collectively suggested that, in absence of epithelial Wnts, blockage of Wnt production from Tagln+ or Acta2+ cells diminished nuclear β-catenin accumulation and canonical Wnt signaling in regenerative epithelial cells.

DISCUSSION

By ablating Wnt secretion from two distinct stromal populations via Tagln-Cre and Acta2-CreER drivers, or from epithelium using Villin-Cre or Villin-CreER, we demonstrated that diminishing Wnt production from either epithelial or these particular stromal subsets compromised the regenerative capability of colonic epithelium. We further showed that aggregated Wnt deprivation from epithelium as well as from Tagln+ or Acta2+ subsets exacerbated the mucosal damage. In addition to documenting previously undescribed role of epithelial Wnts in colonic Reg4 cell differentiation and injury-induced regeneration, our findings supported a model that the accumulated Wnt molecules from multiple tissue sources collected at ISC niche may be critical for injury-induced regeneration.

Literatures documented the growth-driving effects of various Wnts on intestinal stem cell renewal and enteroid growth. Farin et al. and Valenta et al. showed that the addition of Wnt2b was sufficient to restore growth of $Wnt3^{\Delta/\Delta}$ enteroids and *Wls*-deficient enteroids (Farin et al., 2012; Valenta et al., 2016). Wnt5a treatment also resulted in the growth of *Wls*-deficient crypts into small spheroids (Valenta et al., 2016). Kabiri et al. showed that stromal cells promoted survival and growth of *Porcn-deficient* enteroids and supported epithelial regeneration in IEC-specific *Porcn*-deficient mice post-radiation injury (Kabiri et al., 2014). Deleting *Porcn* in telocytes reduced epithelial proliferation in the small and large intestine (Shoshkes-Carmel et al., 2018). Further, mice with Wnt5a deleted in telocytes showed shortened intestines, an observation that was attributed to increased apoptosis in the neonatal mice (Kondo and Kaestner, 2021). Upon infection with rotavirus (RV), an enteric pathogen that affects differentiated cells, the number of CBCs expanded, and the proliferating cells migrated faster. While mice lacking epithelial Wnt did not exhibit a similar response post-infection, suggesting the role of epithelial Wnts in inducing a regenerative response to infection (Zou et al., 2018). In et al. demonstrated a mosaic expression of Wnt2b in specific epithelial cells of human colonic crypts and undifferentiated colonoids. In response to E. coli-secreted cytotoxin EspP-induced injury to colonoids, there was an increase in Wnt2b-expressing cells (In et al., 2020). The infected colonoids failed to survive in the absence of epithelial Wnts when treated with a Porcupine inhibitor, suggesting the importance of epithelial Wnts for colonic regeneration in response to injury. In the context of these studies, we delineated the functional contribution of

Wnts from two uncharacterized stromal populations (Tagln+ and SMA+) to the homeostasis of small and large intestines.

In homeostasis, we found that either constitutive (by *Villin-Cre*) or inducible (by *Villin-CreER*) deletion of epithelial Wls/Gpr177 led to reduction of Reg4+ deep crypt secretory (DCS) cells in the colon, an observation that was not reported before. This change was specific to DCS cells as goblet cells and enterocyte numbers were not affected. DCS cells were originally identified as Paneth cell equivalents that support colonic stem cells (Sasaki et al., 2016). Compared to ablation of epithelial Wnt alone, removing Wnt productions from both epithelium and Tagln+ cells resulted in a near complete blockage of DCS differentiation, suggesting that the differentiation or maturation of colonic DCS cells were proportionally sensitive to a cumulative loss of Wnt availability in the niche. Previous DCS ablation studies documented their indispensable role of maintaining colonic stem cell homeostasis in vivo (Sasaki et al., 2016). Interestingly, the different extent of DCS cell loss in *Gpr177$^{L/L}$;Vil-Cre* and in *Gpr177$^{L/L}$;Vil-Cre;Tagln-Cre* colons positively correlated with different degrees of colonic damages manifested by these DSS-treated homozygotes. Wnt-dependent DCS differentiation identified here offered a mechanism that might contribute to the impaired colonic epithelial repair after Wnt deprivation from epithelial and Tagln+/Acta2+ cell populations.

Bulk RNA-seq and scRNA-seq studies utilized sorted Foxl1+ or Gli1+ cells for transcriptomic analysis (Degirmenci et al., 2018; Shoshkes-Carmel et al., 2018). By contrast, our scRNA study surveyed the intact stroma without selecting or filtering out a specific subepithelial population. The analysis revealed substantial overlaps among Pdgfra+, Gli1+, and Foxl1+, cell clusters, all of which robustly co-expressed Tagln, Acta2, and Myh11. Interestingly, our scRNA analysis also confirmed the Wnt2b expressing Cd81+ Pdgrfa^{lo} cluster (McCarthy et al., 2020), which does not express abundant Tagln, Acta2, and Myh11. 93% of Foxl1 cells expressed Tagln, a gene encoding actin binding protein. Tagln-expressing cells define the widest spectrum of mesenchymal domain including vascular and visceral smooth muscles, myofibroblasts, and fibroblasts (Dong et al., 2012). This mesenchymal cell population was previously shown to regulate intestinal epithelial proliferation and polyposis (Katajisto et al., 2008). We demonstrated that endogenous Tagln+ cells wrapped around crypts in steady-state small intestine and colon. In DSS-treated colon, Tagln+ cells were immediately associated with the regenerating epithelium flanking the wound. Based on our Cre reporter analysis, Tagln-Cre

conceivably targeted more Wnt-producing cells than Acta2-CreER, possibly due to their constitutive versus inducible expression features. In line with this, combined Wnt blockage by Villin-Cre and Tagln-Cre caused the strongest colonic damage, reflected by the highest morbidity and lethality, and a continuous loss of epithelium even in late recovery stage. In addition to chemical injury, we also observed moderately impaired regeneration following irradiation. The stronger impact elicited by DSS could be due to its robust and comprehensive epithelium-damaging effect that was not limited only to cycling ISCs as the irradiation did.

Although Acta2-CreER marked a slightly constrained stromal subset, compared to controls, mice lacking Wnt production from these cells also exhibited a pronounced colonic damage, suggesting that even these smaller stromal subsets actively contributed to epithelial regeneration during injury. Interestingly, this same Acta2 cell population was shown to migrate to colonic wound sites and, when mucosally transplanted, improved colonic epithelial healing after biopsy injury (Manieri et al., 2015). Our data suggested that the presence of Acta2+ cells near epithelial wound may promote colonic healing through Wnt-dependent mechanisms.

Blocking Wnts from Foxl1+ cells caused severe damage to epithelium in both small intestine and colon in unchallenged mice (Shoshkes-Carmel et al., 2018), while blocking Wnts from Gli1+ cells resulted in collapse of colonic crypts and death (Degirmenci et al., 2018). Our scRNA analysis suggested that Foxl1+ cells represented a fraction of Tagln+ domain, and that majority of Foxl1+ cells expressed Tagln. In homeostasis we did not observe a pronounced epithelial damage in small intestines or colons when using various single or combinatory Cre strategies. Our study aligns with the accumulating evidence suggesting that Foxl1+ cells may not function as canonical Wnt producers in spite of expressing Wnt4 and Wnt5a (McCarthy et al., 2020). It is plausible that the Cd81+ Pdgfra^{low} trophocytes, shown to maintain intestinal stem cells *in vivo* (McCarthy et al., 2020), may not effectively deleted by Tagln-Cre and Acta2-CreER drivers reported in this study. Nevertheless, we revealed that blocking Wnt from either Tagln+ or Acta2+ compartment attenuated colonic epithelial regeneration upon DSS injury. Thus, the non-primary Wnt-producing stromal cells also played a role to support injury-induced colonic epithelial regeneration. Taken together, we conclude that the differentiation and regeneration of colonic epithelium were sensitive to the Wnt abundance in ISC niche collected from multiple tissue sources.

Materials and Methods:

Mice and treatment

$Gpr177^{LoxP/LoxP}$ ($Gpr177^{L/L}$), $Gpr177^{+/-}$, Acta2-CreER, Vil-Cre, Villin-CreER mice have been described previously (el Marjou et al., 2004; Fu et al., 2011; Fu et al., 2009; Madison et al., 2002; Manieri et al., 2015). Tagln-Cre mice (Boucher et al., 2003; Holtwick et al., 2002) were obtained from the Jackson Laboratory (Stock #004746). For tamoxifen treatment, adult mice were intraperitoneally injected with a single dose of tamoxifen (75 mg/kg body weight). For total body irradiation, mice were subjected to 12 Gy gamma-irradiation, followed by monitoring of body weight daily. For 5-ethynyl-2'-deoxyuridine (EdU) labeling, EdU (2.5 mg/kg) (Thermo Fisher Scientific, C10338) was injected 30 mins before mice were sacrificed at the indicated days (Yu et al., 2018a). Mice were maintained on a C57BL/6 and 129 mixed background. All experiments were performed on littermates unless explicitly stated in results. Data were quantified from a minimum of three different litters. Numbers of animals used were described in figure legend. All experimental procedures with mice were approved by Rutgers Institutional Animal Care and Use Committee.

Immunohistochemistry and Immunofluorescence staining

Procedures and antibodies for immunohistochemistry and immunofluorescence have been described previously (Das et al., 2015; Feng et al., 2017). In brief, the intestinal tissues were fixed in 4 % PFA at 4 °C overnight, embedded in paraffin, and cut into 5 μm sections. For immunofluorescence staining, the slides were r hydrated, subjected to antigen retrieval (citrate acid buffer, pH 6), and incubated in the blocking buffer (PBS containing 0.1% Triton X-100 with 2% normal serum and 2% BSA) at room temperature for 1 hour. Then the slides were probed with the primary antibodies at 4 °C overnight. Lysozyme (Biogenex, AR024-5R, 1:1), GFP (Invitrogen, A11122 and Abcam, ab6673, 1:500), E-Cadherin (BD Transduction Laboratories, 610182, 1:500), pHH3 (Millipore, 06-570, 1:500), Reg4 (R & D, AF1379, 1:100), Muc2 (Santa Cruz, sc-15334, 1:200), EdU (Thermo Fisher Scientific, C10338), Wnt5a/b (Cell signaling, 2530s), Wnt2b (Abcam, ab50575), and Sm22 (Abcam, ab14106, 1:250) staining were performed according to the manufacturer's instructions. The next day, slides were washed 3 times with PBS and then incubated with Alexus-labeled secondary antibody (Thermo Fisher Scientific, 1:1000) in dark for 1-2 hours. The samples were counterstained with Topro-3

(Thermo Fisher Scientific, T3605, 1:300) and mounted with the ProLong Gold anti-fade mounting media (Thermo Fisher Scientific, P36930). Images were taken using a Zeiss laser scanning microscope. For immunohistochemistry staining, the slides were hydrated, subjected to antigen retrieval (citrate acid buffer, pH 6) and quenched for endogenous peroxidase. The samples were incubated in the blocking buffer at room temperature for 1 hour and then incubated with Lysozyme (Biogenex, AR024-5R, 1:8), β-catenin (BD Transduction Laboratories, 610153, 1:1000), PCNA (Santa Cruz, sc-56, 1:1000), c-Myc (Millipore Sigma, CBL430, 1:100), CD44 (Cell signaling, 3570, 1:100), and Axin2 (Thermo Fisher Scientific, MA5-32646, 1:100) at 4 °C overnight. The next day, slides were washed 3 times with PBS and then incubated with Biotin-labeled secondary antibody (Vector-Lab, 1:500) for 1-2 hours. Staining was developed using an ABC Kit (Vector Lab, PK-6100) and followed by the DAB kit (Vector-Lab, SK-4100). The samples were counterstained with hematoxylin (Vector-Lab, H-3404) and mounted with cytoseal mounting media (Thermo Fisher Scientific, 8310-4). Images were taken under the Nikon (TE2000-U) light microscope.

Quantitative real-time PCR

Quantitative RT-PCR has been described earlier (Das et al., 2015; Gao and Kaestner, 2010; Gao et al., 2009; Sakamori et al., 2012; Sakamori et al., 2014), with a list of primers provided in Table 1. Threshold cycle (Ct) values obtained for each gene were normalized to Ct values obtained for either *beta-actin* or *Hypoxanthine-guanine phosphoribosyl transferase (Hprt)*. Data was obtained from 3 independent biological samples with 3 technical replicates.

RNA in situ hybridization

The procedure was followed as previously described (Gregorieff and Clevers, 2010), with the following modifications. In brief, cryo-sections were cut at 8 µm, thawed at room temperature (RT) for 15 minutes and post-fixed in 4 %PFA. After incubating the tissue sections in 0.25 % acetic anhydride solution, the sections were incubated in the hybridization solution with the probes, as mentioned below, for 24-48 hrs. The concentration of *Olfm4* probe is 1 µg/ml and *Gpr177* probe is 2 µg/ml. The sections were incubated with antibody over night at 4 °C and then in BM-Purple (Roche, Catalog# 11 442 074 001) for up to 24 hrs in the dark. Slides were counter stained with Nuclear Fast Red (Vector Lab, H-3403) and mounted with Cytoseal

mounting media (Thermo Fisher Scientific, 8310-4). Images were taken with the Nikon (TE2000-U) light microscope.

Organoid Culture

Procedures for crypt isolation and organoid culture were as previously described (Das et al., 2015; Sato and Clevers, 2013; Sato et al., 2009). Organoids isolated from $Gpr177^{L/L}$ Vil-Cre mice were cultured in ENR media for 7 days and counted daily. Wnt3a (100 ng/ml and 200 ng/ml) and CHIR (3 μM) were added to the ENR media at day 1. Organoids isolated from $Gpr177^{L/}$; Vil-CreER mice were cultured in ENR media for 5 days. Vehicle or 4-OHT (0.5 μM) was added to the media for 12 hrs on day 6. The organoids were then cultured in ENR media without or with Wnt3a (100 ng/ml)The organoids were counted daily and imaged on day 6. EdU (10 μm) was added into the culture media for 30 min on day 6. The organoids were fixed in 4 % PFA and the EdU staining was performed according to the manufacturer's instructions.

DSS-induced experimental colitis

The mice were administered with 2.5% dextran sulfate sodium (DSS, Colitis grade, 36-50KDa, MP Biologics, SKU 0216011080) in tap water for 7 days and recovered with tap water for another 7 days. The body weight of individual mice was monitored daily and the graph was plotted using GraphPad Prism version 8.3. Colon tissues were harvested for pathological analysis. Colonic damage was scored blindly by a GI pathologist as described previously (Chassaing et al., 2014) in Figures 6E and 6I. Briefly, scores (0-4) were assigned based on the severity of epithelial injury and leukocyte infiltration into the mucosa, submucosa and muscularis. These three scores were multiplied by an extended factor to assess the extent of the change: 1 for focal, 2 for patchy, and 3 for diffuse, and summed to achieve the final score out of the maximal score of 36. In Supplementary figure 5, colitis scoring was performed by an independent experimentalist using a different method described previously (Chinen et al., 2011)

Single cell dissociation and sorting

The distal ileum of a wild-type mouse was harvested and briefly rinsed in ice-cold PBS (Fisher Scientific, SH30256LS). The tissue was opened longitudinally, rinsed in ice-cold PBS, and further sliced to 1-2 mm pieces. The pieces were rinsed in 30mL of ice-cold PBS by inverting

the falcon tube 10-15 times. The pieces were then transferred into fresh 30ml of ice-cold PBS. This step was repeated until the solution remained clear after inverting. Each piece was then transferred to 30 mL crypt isolation buffer, containing 5 mM EDTA [Invitrogen, AM9260G], 2% BSA [Sigma, A3294], and HBSS Ca/Mg-free [Sigma, H9394], and allowed to shake at 37˚C for 15 minutes. The tube was subsequently vigorously shaken to release the epithelial layer from the pieces after which the solution was discarded. This was repeated in another 30ml of crypt isolation buffer. The pieces were then incubated in DMEM/F12 medium (ThermoFisher, 12634-010) for 10 minutes on a petri dish, at room temperature. The solution was discarded, and the pieces were thoroughly minced. 10ml of digestion buffer (100 U/mL Collagenase II [ThermoFisher, 17101015], 500 U/mL DNase I [Qiagen, 79254], and HBSS Ca/Mg free) was added to the minced tissue and allowed to shake at 37˚C for 30 minutes. The tissue was completely digested, and the solution was passed through a 70µM cell strainer into a 50mL falcon tube. The tube was centrifuged at 200g for 10 minutes. The pellet was resuspended in 1mL of FACS solution (2% BSA in PBS). The single-cell suspensions were stained with DAPI prior to sorting. Single-cell suspensions were subjected to sorting by BD Biosciences Aria II Flow Cytometer (BD FACSAria II). Single viable lamina propria lymphocytes and mesenchymal cells were gated by forward scatter, side scatter and by negative staining for DAPI.

Droplet-based scRNA-Seq

Cell number and viability were determined by a Propidium Iodide based fluorescence assay using Moxi GO II System, Orflo Prod#MXG102 (ORFLO Technologies, LLC). Droplet-based single-cell partitioning and single-cell RNA-Seq libraries were generated using the Chromium Single-Cell 3′ Reagent v3 Kit (10X Genomics, Pleasanton, CA) on the 10X Chromium Controller as per the manufacturer's protocol. Live cells in single cell suspension with 95% viability were mixed with Gel beads, RT reagents and Partitioning Oil into a Single-Cell 3′ Chip and loaded onto 10X Chromium Controller for GEM generation. Briefly, the protocol includes RT, cleanup, cDNA amplification, fragmentation, end repair & A-tail prep, adapter ligation and incorporation of sample indices into finished libraries, which are compatible with Illumina next-generation sequencing platforms. Sample quantification and quality control were determined using Qubit Fluorometer (Invitrogen, Life Technologies) and TapeStation (Agilent Technologies, Santa Clara CA) respectively. cDNA libraries were sequenced on Illumina NovaSeq 6000

sequencer (Illumina, San Diego, CA) with a configuration of 28/8/0/91-bp for cell barcode, sample barcode and mRNA reads respectively as recommendation by 10X Genomics. The Chromium Single Cell Software is used to analyze and visualize single cell 3' RNA-seq data produced by the 10X Chromium Platform. The 10X chromium software package includes Cell Ranger Pipelines and Loupe Cell Browser. Cell Ranger pipelines use raw 10X single cell sequencing data from an Illumina sequencer and perform demultiplexing, unique barcode processing, and single cell 3' gene counting.

For Figures 2A-D, the WT count matrix files generated by Cell Ranger was transformed into the count matrix by R (version 3.6.1). Count matrices for different groups were combined and used as the input for Seurat package (version 3.1.0) (Butler et al., 2018; Stuart et al., 2019). Data normalization was performed by Seurat using the "LogNormalize" method. Briefly, the gene counts for each cell were divided by the total counts for that cell and multiplied by the scale factor (10000). The data was then natural log transformed. Cells with less than 200 expressed genes and genes expressed in less than 3 cells were removed from the downstream analyses. The top 2000 variable genes were used to perform PCA (primary component analysis). 10 out of 20 PCs were selected for doing clustering and Uniform Manifold Approximation and Projection (UMAP). DE(differential expression) was performed by Seurat using the Wilcoxon test. DEGs with p-value <= 0.05, logFC > 0.2, and percentage of expression in each group >0.25 and were visualized by generating a heat map. Based on the expression of Wnts indicated in figure 2B, clusters 4, 9, 11, 14, and 21 were further selected to visualize the expression of key Wnts and stromal markers mentioned in figure 2C.

For supplemental figures 2A-B, Single Cell Deep Constrained Clustering (scDCC) was performed for Wnt4 and Wnt5a. The top 2000 most highly variable genes were identified using Seurat with the selection method of vst that calculates feature variance by fitting the variance-mean relationship. Then the expression data of these genes was fed to **scDCC. scDCC** is a deep learning model that requires two inputs: expression data and marker genes. In this study, **scDCC** was based on marker genes Wnt4 and Wnt5a. The restriction of binding genes was based on their distances from each other. If the distance between two genes was among the top 10% farthest distances, they were marked as not being connected, while if their distance

was smaller than 90% of distances of other gene pairs, they were marked as must be connected. After **scDCC** reduced the dimensions of the scRNA-seq data, **t-SNE** was applied for visualization.

For Figures 2E-F, and Supplemental Figures 2C-G, the WT count matrix file generated by Cell Ranger was imported to Partek flow software for secondary data analysis. The single cell analysis was generated using Partek® Flow®, version 9.0, build 9.0.20.0202. Copyright ©; 2020 Partek Inc., St. Louis, MO, USA. For each cell, quality control metrics such as number of read counts, number of detected genes, and percentage of mitochondrial reads were calculated and used to filter out low quality cells. The data was then log2+1 normalized based on counts per million and the genes that were not expressed in at least 99% of the cells were excluded from the data set. Principal components (PCs) were calculated for the samples and the scree plot was used to determine the number of PCs to be used. Based on the PC value, cells were divided into clusters in an unsupervised fashion. The ANOVA test was used to identify differentially expressed genes (DEGs) for each cluster by comparing genes in all the clusters, filtering genes that were upregulated by 1.5-fold, and then sorting them by ascending p-value. The clusters were then visualized using t-Distributed Stochastic Neighbor Embedding (t-SNE). Based on the expression of Tagln and Foxl1, the cells were selected and classified. DEGs were identified for the three populations- Foxl1-/Tagln+, Foxl1+/Tagln+, and Foxl1+/Tagln- and the signature DEG genes (FDR set up ≤1e-8, fold change>2) were visualized by generating a heat map and by generating violin plots for genes of interest.

Transmission EM analysis and Gpr177 immunogold labeling

TEM procedures have been described previously (Gao and Kaestner, 2010; Sakamori et al., 2012). For Gpr177 immunogold labeling and EM analysis, duodenal and jejunal tissues were dissected from wild type and Gpr177$^{L/}$; Vil-Cre mice and immediately fixed as ~1 mm fragments in 2.5% paraformaldehyde in cacodylate buffer, pH 7.4 overnight. The tissue was then sliced to 100-200 microns thickness on a vibratome and frozen between two brass “top-hats” in a HPM010 (Abra Fluid AG. 45 Widnau, Switerlan) at 5,000 P.S.I. at -180 °C. Next, the frozen tissue was transferred to frozen glass-distilled 100% acetone and dehydrated at -90 °C for 48 hours. The tissue was then infiltrated with HM-20 lowicryl and polymerized with 360 nm

light at -50 °C in a dry nitrogen environment. Tissue sections cut 60 nm thick containing Paneth cells were immunolabeled with Gpr177 antibody (Fu et al., 2009) at 1:250 to 1:50 in 5% BSA, 0.1% cold water fish gelatin in PBS pH 7.4. No primary antibody control and *Gpr177*-deficient cells were used in initial tests to optimize labeling conditions. Images shown were immunolabeled with 1:100 dilution of primary antibody. Stable antigen-antibody complexes were detected with protein A conjugated to either 15nm gold colloids or 20nm gold colloids. Imaging was performed with a FEI Tecnai-12 microscope at 80 keV using a nominal magnification of 6500×. Montage images were collected using Serial EM and stitched together with the IMOD subroutine Blendmont (Kremer et al., 1996; Mastronarde, 2005). Each image has a pixel dimension of ~3 nm such that each spherical gold particle should fill 5 pixels and resizing of the images should provide information to reveal the approximate volume the gold would occupy in the images. Immunogold particles were counted manually, excluding particles within nuclear area. Area and perimeter of individual Paneth cells were measured using Photoshop CS. Number of immunogold particles in each subcellular compartment per unit area (for ER and Golgi) or per unit length (for plasma membrane) were calculated and compared by t-test.

Quantifications and statistical analyses

Quantification was made from at least three animals per genotype for each experiment as previously described (Das et al., 2015; Feng et al., 2017). All comparisons were made among littermates. 50-100 crypts of small intestine and about 50 colonic crypts were counted per marker per genotype. For the number of regenerative crypts, all crypts were counted within 50 villi regardless of their sectioned shape. Length of wound were measured along multiple wound beds by Image J and the average length were calculated. Statistical significance was analyzed using Student's t test, two-tailed, unpaired, or one-way ANOVA. *, $p < 0.05$; **, $p < 0.01$; ***, $p < 0.001$. In Fig. 2, the statistical significance for body weights was analyzed using two-way ANOVA and the survival curve was analyzed using Gehan-Breslow-Wilcoxon test. Graphs were made using GraphPad Prism version 7.02, 8.3, and 9.

Data Availability

The scRNA seq data has been deposited in the GEO database (GSE151152).

For further information, please refer to the Supplementary Materials and Methods.

ACKNOWLEDGEMENT:

This work was supported by: NIH grants (R01DK102934, R01AT010243, R01DK119198), American Cancer Society Scholar Award (RSG-15-060-01-TBE), NSF/BIO/IDBR grants (1353890, 195282), and a Rutgers IMRT award to N.G.; NIH grants (R01DE015654, R01DE026936) to W.H.; New Jersey Commission on Cancer Research Postdoctoral Fellowship (DFHS16PPC045) to Q.F.

References

<2009 PNAS Fu et al Gpr177 paper.pdf>.

Angers, S. and Moon, R. T. (2009). Proximal events in Wnt signal transduction. *Nat Rev Mol Cell Biol* **10**, 468-477.

Aoki, R., Shoshkes-Carmel, M., Gao, N., Shin, S., May, C. L., Golson, M. L., Zahm, A. M., Ray, M., Wiser, C. L., Wright, C. V., et al. (2016). Foxl1-expressing mesenchymal cells constitute the intestinal stem cell niche. *Cell Mol Gastroenterol Hepatol* **2**, 175-188.

Banziger, C., Soldini, D., Schutt, C., Zipperlen, P., Hausmann, G. and Basler, K. (2006). Wntless, a conserved membrane protein dedicated to the secretion of Wnt proteins from signaling cells. *Cell* **125**, 509-522.

Barker, N., van Es, J. H., Kuipers, J., Kujala, P., van den Born, M., Cozijnsen, M., Haegebarth, A., Korving, J., Begthel, H., Peters, P. J., et al. (2007). Identification of stem cells in small intestine and colon by marker gene Lgr5. *Nature* **449**, 1003-1007.

Bartscherer, K., Pelte, N., Ingelfinger, D. and Boutros, M. (2006). Secretion of Wnt ligands requires Evi, a conserved transmembrane protein. *Cell* **125**, 523-533.

Bohin, N., Carlson, E. A. and Samuelson, L. C. (2018). Genome Toxicity and Impaired Stem Cell Function after Conditional Activation of CreER(T2) in the Intestine. *Stem Cell Reports* **11**, 1337-1346.

Boucher, P., Gotthardt, M., Li, W. P., Anderson, R. G. and Herz, J. (2003). LRP: role in vascular wall integrity and protection from atherosclerosis. *Science* **300**, 329-332.

Boutros, M. and Mlodzik, M. (1999). Dishevelled: at the crossroads of divergent intracellular signaling pathways. *Mech Dev* **83**, 27-37.

Butler, A., Hoffman, P., Smibert, P., Papalexi, E. and Satija, R. (2018). Integrating single-cell transcriptomic data across different conditions, technologies, and species. *Nat Biotechnol* **36**, 411-420.

Cadigan, K. M. and Peifer, M. (2009). Wnt signaling from development to disease: insights from model systems. *Cold Spring Harb Perspect Biol* **1**, a002881.

Chassaing, B., Aitken, J. D., Malleshappa, M. and Vijay-Kumar, M. (2014). Dextran sulfate sodium (DSS)-induced colitis in mice. *Curr Protoc Immunol* **104**, Unit 15 25.

Chinen, T., Komai, K., Muto, G., Morita, R., Inoue, N., Yoshida, H., Sekiya, T., Yoshida, R., Nakamura, K., Takayanagi, R., et al. (2011). Prostaglandin E2 and SOCS1 have a role in intestinal immune tolerance. *Nature communications* **2**, 190.

Ching, W. and Nusse, R. (2006). A dedicated Wnt secretion factor. *Cell* **125**, 432-433.

Clevers, H. and Nusse, R. (2012). Wnt/β-catenin signaling and disease. *Cell* **149**, 1192-1205.

Das, S., Yu, S., Sakamori, R., Stypulkowski, E. and Gao, N. (2012). Wntless in Wnt secretion: molecular, cellular and genetic aspects. *Front Biol (Beijing)* **7**, 587-593.

Das, S., Yu, S., Sakamori, R., Vedula, P., Feng, Q., Flores, J., Hoffman, A., Fu, J., Stypulkowski, E., Rodriguez, A., et al. (2015). Rab8a vesicles regulate Wnt ligand delivery and Paneth cell maturation at the intestinal stem cell niche. *Development* **142**, 2147-2162.

de Groot, R. E., Farin, H. F., Macurkova, M., van Es, J. H., Clevers, H. C. and Korswagen, H. C. (2013). Retromer dependent recycling of the Wnt secretion factor Wls is dispensable for stem cell maintenance in the mammalian intestinal epithelium. *PLoS One* **8**, e76971.

de Lau, W., Barker, N. and Clevers, H. (2007). WNT signaling in the normal intestine and colorectal cancer. *Front Biosci* **12**, 471-491.

Degirmenci, B., Valenta, T., Dimitrieva, S., Hausmann, G. and Basler, K. (2018). GLI1-expressing mesenchymal cells form the essential Wnt-secreting niche for colon stem cells. *Nature* **558**, 449-453.

Dong, L. H., Lv, P. and Han, M. (2012). Roles of SM22alpha in cellular plasticity and vascular diseases. *Cardiovasc Hematol Disord Drug Targets* **12**, 119-125.

Eaton, S., Wepf, R. and Simons, K. (1996). Roles for Rac1 and Cdc42 in planar polarization and hair outgrowth in the wing of Drosophila. *J Cell Biol* **135**, 1277-1289.

el Marjou, F., Janssen, K. P., Chang, B. H., Li, M., Hindie, V., Chan, L., Louvard, D., Chambon, P., Metzger, D. and Robine, S. (2004). Tissue-specific and inducible Cre-mediated recombination in the gut epithelium. *Genesis* **39**, 186-193.

Fanto, M., Weber, U., Strutt, D. I. and Mlodzik, M. (2000). Nuclear signaling by Rac and Rho GTPases is required in the establishment of epithelial planar polarity in the Drosophila eye. *Curr Biol* **10**, 979-988.

Farin, H. F., Van Es, J. H. and Clevers, H. (2012). Redundant Sources of Wnt Regulate Intestinal Stem Cells and Promote Formation of Paneth Cells. *Gastroenterology* **143**, 1518-1529.

Feng, Q., Bonder, E. M., Engevik, A. C., Zhang, L., Tyska, M. J., Goldenring, J. R. and Gao, N. (2017). Disruption of Rab8a and Rab11a causes formation of basolateral microvilli in neonatal enteropathy. *J Cell Sci*.

Fevr, T., Robine, S., Louvard, D. and Huelsken, J. (2007). Wnt/beta-catenin is essential for intestinal homeostasis and maintenance of intestinal stem cells. *Mol Cell Biol* **27**, 7551-7559.

Fu, J., Ivy Yu, H. M., Maruyama, T., Mirando, A. J. and Hsu, W. (2011). Gpr177/mouse Wntless is essential for Wnt-mediated craniofacial and brain development. *Dev Dyn* **240**, 365-371.

Fu, J., Jiang, M., Mirando, A. J., Ivy Yu, H. M. and Hsu, W. (2009). Reciprocal regulation of Wnt and Gpr177/mouse Wntless is required for embryonic axis formation. *PNAS* **106**, 18598-18603.

Gao, N. and Kaestner, K. H. (2010). Cdx2 regulates endo-lysosomal function and epithelial cell polarity. *Genes Dev* **24**, 1295-1305.

Gao, N., White, P. and Kaestner, K. H. (2009). Establishment of intestinal identity and epithelial-mesenchymal signaling by Cdx2. *Dev Cell* **16**, 588-599.

Gregorieff, A. and Clevers, H. (2010). In situ hybridization to identify gut stem cells. *Curr Protoc Stem Cell Biol* **Chapter 2**, Unit 2F 1.

Gregorieff, A., Pinto, D., Begthel, H., Destree, O., Kielman, M. and Clevers, H. (2005). Expression pattern of Wnt signaling components in the adult intestine. *Gastroenterology* **129**, 626-638.

Greicius, G., Kabiri, Z., Sigmundsson, K., Liang, C., Bunte, R., Singh, M. K. and Virshup, D. M. (2018). PDGFRalpha(+) pericryptal stromal cells are the critical source of Wnts and RSPO3 for murine intestinal stem cells in vivo. *Proc Natl Acad Sci U S A* **115**, E3173-E3181.

Habas, R., Dawid, I. B. and He, X. (2003). Coactivation of Rac and Rho by Wnt/Frizzled signaling is required for vertebrate gastrulation. *Genes Dev* **17**, 295-309.

Habas, R., Kato, Y. and He, X. (2001). Wnt/Frizzled activation of Rho regulates vertebrate gastrulation and requires a novel Formin homology protein Daam1. *Cell* **107**, 843-854.

He, X., Semenov, M., Tamai, K. and Zeng, X. (2004). LDL receptor-related proteins 5 and 6 in Wnt/beta-catenin signaling: arrows point the way. *Development* **131**, 1663-1677.

Holtwick, R., Gotthardt, M., Skryabin, B., Steinmetz, M., Potthast, R., Zetsche, B., Hammer, R. E., Herz, J. and Kuhn, M. (2002). Smooth muscle-selective deletion of guanylyl cyclase-A prevents the acute but not chronic effects of ANP on blood pressure. *Proc Natl Acad Sci U S A* **99**, 7142-7147.

Huang, H. and He, X. (2008). Wnt/beta-catenin signaling: new (and old) players and new insights. *Curr Opin Cell Biol* **20**, 119-125.

Huh, W. J., Mysorekar, I. U. and Mills, J. C. (2010). Inducible activation of Cre recombinase in adult mice causes gastric epithelial atrophy, metaplasia, and regenerative changes in the absence of "floxed" alleles. *Am J Physiol Gastrointest Liver Physiol* **299**, G368-380.

Kabiri, Z., Greicius, G., Madan, B., Biechele, S., Zhong, Z., Zaribafzadeh, H., Edison, Aliyev, J., Wu, Y., Bunte, R., et al. (2014). Stroma provides an intestinal stem cell niche in the absence of epithelial Wnts. *Development* **141**, 2206-2215.

Katajisto, P., Vaahtomeri, K., Ekman, N., Ventela, E., Ristimaki, A., Bardeesy, N., Feil, R., DePinho, R. A. and Makela, T. P. (2008). LKB1 signaling in mesenchymal cells required for suppression of gastrointestinal polyposis. *Nat Genet* **40**, 455-459.

Koch, S., Nava, P., Addis, C., Kim, W., Denning, T. L., Li, L., Parkos, C. A. and Nusrat, A. (2011). The Wnt antagonist Dkk1 regulates intestinal epithelial homeostasis and wound repair. *Gastroenterology* **141**, 259-268, 268 e251-258.

Korinek, V., Barker, N., Moerer, P., Donselaar, E. V., Huls, G., Peters, P. J. and Clevers, H. (1998). Depletion of epithelial stem-cell compartments in the small intestine of mice lacking Tcf-4. *Nature genetics* **19**, 379-383.

Kuhbandner, S., Brummer, S., Metzger, D., Chambon, P., Hofmann, F. and Feil, R. (2000). Temporally controlled somatic mutagenesis in smooth muscle. *Genesis* **28**, 15-22.

Kuhnert, F., Davis, C. R., Wang, H. T., Chu, P., Lee, M., Yuan, J., Nusse, R. and Kuo, C. J. (2004). Essential requirement for Wnt signaling in proliferation of adult small intestine and colon revealed by adenoviral expression of Dickkopf-1. *Proceedings of the National Academy of Sciences of the United States of America* **101**, 266-271.

MacDonald, B. T. and He, X. (2012). Frizzled and LRP5/6 receptors for Wnt/β-catenin signaling. *Cold Spring Harb Perspect Biol* **4**.

MacDonald, B. T., Tamai, K. and He, X. (2009). Wnt/beta-catenin signaling: components, mechanisms, and diseases. *Dev Cell* **17**, 9-26.

Madison, B. B., Dunbar, L., Qiao, X. T., Braunstein, K., Braunstein, E. and Gumucio, D. L. (2002). Cis elements of the villin gene control expression in restricted domains of the vertical (crypt) and horizontal (duodenum, cecum) axes of the intestine. *J Biol Chem* **277**, 33275-33283.

Manieri, N. A., Mack, M. R., Himmelrich, M. D., Worthley, D. L., Hanson, E. M., Eckmann, L., Wang, T. C. and Stappenbeck, T. S. (2015). Mucosally transplanted mesenchymal stem cells stimulate intestinal healing by promoting angiogenesis. *J Clin Invest* **125**, 3606-3618.

McCarthy, N., Manieri, E., Storm, E. E., Saadatpour, A., Luoma, A. M., Kapoor, V. N., Madha, S., Gaynor, L. T., Cox, C., Keerthivasan, S., et al. (2020). Distinct Mesenchymal Cell Populations Generate the Essential Intestinal BMP Signaling Gradient. *Cell Stem Cell* **26**, 391-402 e395.

Miyoshi, H., Ajima, R., Luo, C. T., Yamaguchi, T. P. and Stappenbeck, T. S. (2012). Wnt5a potentiates TGF-beta signaling to promote colonic crypt regeneration after tissue injury. *Science* **338**, 108-113.

Nusse, R., Fuerer, C., Ching, W., Harnish, K., Logan, C., Zeng, A., ten Berge, D. and Kalani, Y. (2008). Wnt signaling and stem cell control. *Cold Spring Harb Symp Quant Biol* **73**, 59-66.

Pinto, D., Gregorieff, A., Begthel, H. and Clevers, H. (2003). Canonical Wnt signals are essential for homeostasis of the intestinal epithelium. *Genes Dev* **17**, 1709-1713.

Polakis, P. (2007). The many ways of Wnt in cancer. *Curr Opin Genet Dev* **17**, 45-51.

Port, F. and Basler, K. (2010). Wnt trafficking: new insights into Wnt maturation, secretion and spreading. *Traffic* **11**, 1265-1271.

Potten, C. S. (1977). Extreme sensitivity of some intestinal crypt cells to X and γ irradiation. *Nature* **269**, 518.

Powell, D. W., Pinchuk, I. V., Saada, J. I., Chen, X. and Mifflin, R. C. (2011). Mesenchymal cells of the intestinal lamina propria. *Annu Rev Physiol* **73**, 213-237.

Reya, T. and Clevers, H. (2005). Wnt signalling in stem cells and cancer. *Nature* **434**, 843-850.

Saha, S., Aranda, E., Hayakawa, Y., Bhanja, P., Atay, S., Brodin, N. P., Li, J., Asfaha, S., Liu, L., Tailor, Y., et al. (2016). Macrophage-derived extracellular vesicle-packaged WNTs rescue intestinal stem cells and enhance survival after radiation injury. *Nature communications* **7**, 13096.

Sakamori, R., Das, S., Yu, S., Feng, S., Stypulkowski, E., Guan, Y., Douard, V., Tang, W., Ferraris, R. P., Harada, A., et al. (2012). Cdc42 and Rab8a are critical for intestinal stem cell division, survival, and differentiation in mice. *J Clin Invest* **122**, 1052-1065.

Sakamori, R., Yu, S., Zhang, X., Hoffman, A., Sun, J., Das, S., Vedula, P., Li, G., Fu, J., Walker, F., et al. (2014). CDC42 Inhibition Suppresses Progression of Incipient Intestinal Tumors. *Cancer Res* **74**, 5480-5492.

San Roman, A. K., Jayewickreme, C. D., Murtaugh, L. C. and Shivdasani, R. A. (2014). Wnt secretion from epithelial cells and subepithelial myofibroblasts is not required in the mouse intestinal stem cell niche in vivo. *Stem Cell Reports* **2**, 127-134.

Sasaki, N., Sachs, N., Wiebrands, K., Ellenbroek, S. I., Fumagalli, A., Lyubimova, A., Begthel, H., van den Born, M., van Es, J. H., Karthaus, W. R., et al. (2016). Reg4+ deep crypt secretory cells function as epithelial niche for Lgr5+ stem cells in colon. *Proc Natl Acad Sci U S A* **113**, E5399-5407.

Sato, T. and Clevers, H. (2013). Primary mouse small intestinal epithelial cell cultures. *Methods Mol Biol* **945**, 319-328.

Sato, T., van Es, J. H., Snippert, H. J., Stange, D. E., Vries, R. G., van den Born, M., Barker, N., Shroyer, N. F., van de Wetering, M. and Clevers, H. (2011). Paneth cells constitute the niche for Lgr5 stem cells in intestinal crypts. *Nature* **469**, 415-418.

Sato, T., Vries, R. G., Snippert, H. J., van de Wetering, M., Barker, N., Stange, D. E., van Es, J. H., Abo, A., Kujala, P., Peters, P. J., et al. (2009). Single Lgr5 stem cells build crypt-villus structures in vitro without a mesenchymal niche. *Nature* **459**, 262-265.

Schulte, G. (2010). International Union of Basic and Clinical Pharmacology. LXXX. The class Frizzled receptors. *Pharmacol Rev* **62**, 632-667.

Schulte, G. and Bryja, V. (2007). The Frizzled family of unconventional G-protein-coupled receptors. *Trends Pharmacol Sci* **28**, 518-525.

Shoshkes-Carmel, M., Wang, Y. J., Wangensteen, K. J., Toth, B., Kondo, A., Massasa, E. E., Itzkovitz, S. and Kaestner, K. H. (2018). Subepithelial telocytes are an important source of Wnts that supports intestinal crypts. *Nature* **557**, 242-246.

Srinivas, S., Watanabe, T., Lin, C. S., William, C. M., Tanabe, Y., Jessell, T. M. and Costantini, F. (2001). Cre reporter strains produced by targeted insertion of EYFP and ECFP into the ROSA26 locus. *BMC Dev Biol* **1**, 4.

Strutt, D. I., Weber, U. and Mlodzik, M. (1997). The role of RhoA in tissue polarity and Frizzled signalling. *Nature* **387**, 292-295.

Stuart, T., Butler, A., Hoffman, P., Hafemeister, C., Papalexi, E., Mauck, W. M., 3rd, Hao, Y., Stoeckius, M., Smibert, P. and Satija, R. (2019). Comprehensive Integration of Single-Cell Data. *Cell* **177**, 1888-1902 e1821.

Stzepourginski, I., Nigro, G., Jacob, J. M., Dulauroy, S., Sansonetti, P. J., Eberl, G. and Peduto, L. (2016). CD34+ mesenchymal cells are a major component of the intestinal stem cells niche at homeostasis and after injury. *Proc Natl Acad Sci U S A* **114**, E506-E513.

Takada, R., Satomi, Y., Kurata, T., Ueno, N., Norioka, S., Kondoh, H., Takao, T. and Takada, S. (2006). Monounsaturated fatty acid modification of Wnt protein: its role in Wnt secretion. *Developmental cell* **11**, 791-801.

Tamai, K., Semenov, M., Kato, Y., Spokony, R., Liu, C., Katsuyama, Y., Hess, F., Saint-Jeannet, J. P. and He, X. (2000). LDL-receptor-related proteins in Wnt signal transduction. *Nature* **407**, 530-535.

Valenta, T., Degirmenci, B., Moor, A. E., Herr, P., Zimmerli, D., Moor, M. B., Hausmann, G., Cantu, C., Aguet, M. and Basler, K. (2016). Wnt Ligands Secreted by Subepithelial Mesenchymal Cells Are Essential for the Survival of Intestinal Stem Cells and Gut Homeostasis. *Cell Rep* **15**, 911-918.

van de Wetering, M., Sancho, E., Verweij, C., de Lau, W., Oving, I., Hurlstone, A., van der Horn, K., Batlle, E., Coudreuse, D., Haramis, A. P., et al. (2002). The beta-catenin/TCF-4 complex imposes a crypt progenitor phenotype on colorectal cancer cells. *Cell* **111**, 241-250.

van Es, J. H., Haegebarth, A., Kujala, P., Itzkovitz, S., Koo, B. K., Boj, S. F., Korving, J., van den Born, M., van Oudenaarden, A., Robine, S., et al. (2012). A critical role for the Wnt effector Tcf4 in adult intestinal homeostatic self-renewal. *Mol Cell Biol* **32**, 1918-1927.

Wallingford, J. B. and Habas, R. (2005). The developmental biology of Dishevelled: an enigmatic protein governing cell fate and cell polarity. *Development* **132**, 4421-4436.

Wehrli, M., Dougan, S. T., Caldwell, K., O'Keefe, L., Schwartz, S., Vaizel-Ohayon, D., Schejter, E., Tomlinson, A. and DiNardo, S. (2000). arrow encodes an LDL-receptor-related protein essential for Wingless signalling. *Nature* **407**, 527-530.

Willert, K., Brown, J. D., Danenberg, E., Duncan, A. W., Weissman, I. L., Reya, T., Yates, J. R. and Nusse, R. (2003). Wnt proteins are lipid-modified and can act as stem cell growth factors. *Nature* **423**, 448-452.

Willert, K. and Nusse, R. (2012). Wnt proteins. *Cold Spring Harb Perspect Biol* **4**, a007864.

Wu, C. H. and Nusse, R. (2002). Ligand receptor interactions in the Wnt signaling pathway in Drosophila. *J Biol Chem* **277**, 41762-41769.

Yan, K. S., Janda, C. Y., Chang, J., Zheng, G. X. Y., Larkin, K. A., Luca, V. C., Chia, L. A., Mah, A. T., Han, A., Terry, J. M., et al. (2017). Non-equivalence of Wnt and R-spondin ligands during Lgr5(+) intestinal stem-cell self-renewal. *Nature* **545**, 238-242.

Yu, S., Balasubramanian, I., Laubitz, D., Tong, K., Bandyopadhyay, S., Lin, X., Flores, J., Singh, R., Liu, Y., Macazana, C., et al. (2020). Paneth Cell-Derived Lysozyme Defines the Composition of Mucolytic Microbiota and the Inflammatory Tone of the Intestine. *Immunity* **53**, 398-416 e398.

Yu, S., Tong, K., Zhao, Y., Balasubramanian, I., Yap, G. S., Ferraris, R. P., Bonder, E. M., Verzi, M. P. and Gao, N. (2018a). Paneth Cell Multipotency Induced by Notch Activation following Injury. *Cell Stem Cell*.

---- (2018b). Paneth Cell Multipotency Induced by Notch Activation following Injury. *Cell Stem Cell* **23**, 46-59 e45.

Zhang, X., Bandyopadhyay, S., Araujo, L. P., Tong, K., Flores, J., Laubitz, D., Zhao, Y., Yap, G., Wang, J., Zou, Q., et al. (2020). Elevating EGFR-MAPK program by a nonconventional Cdc42 enhances intestinal epithelial survival and regeneration. *JCI Insight* **5**.

Figures

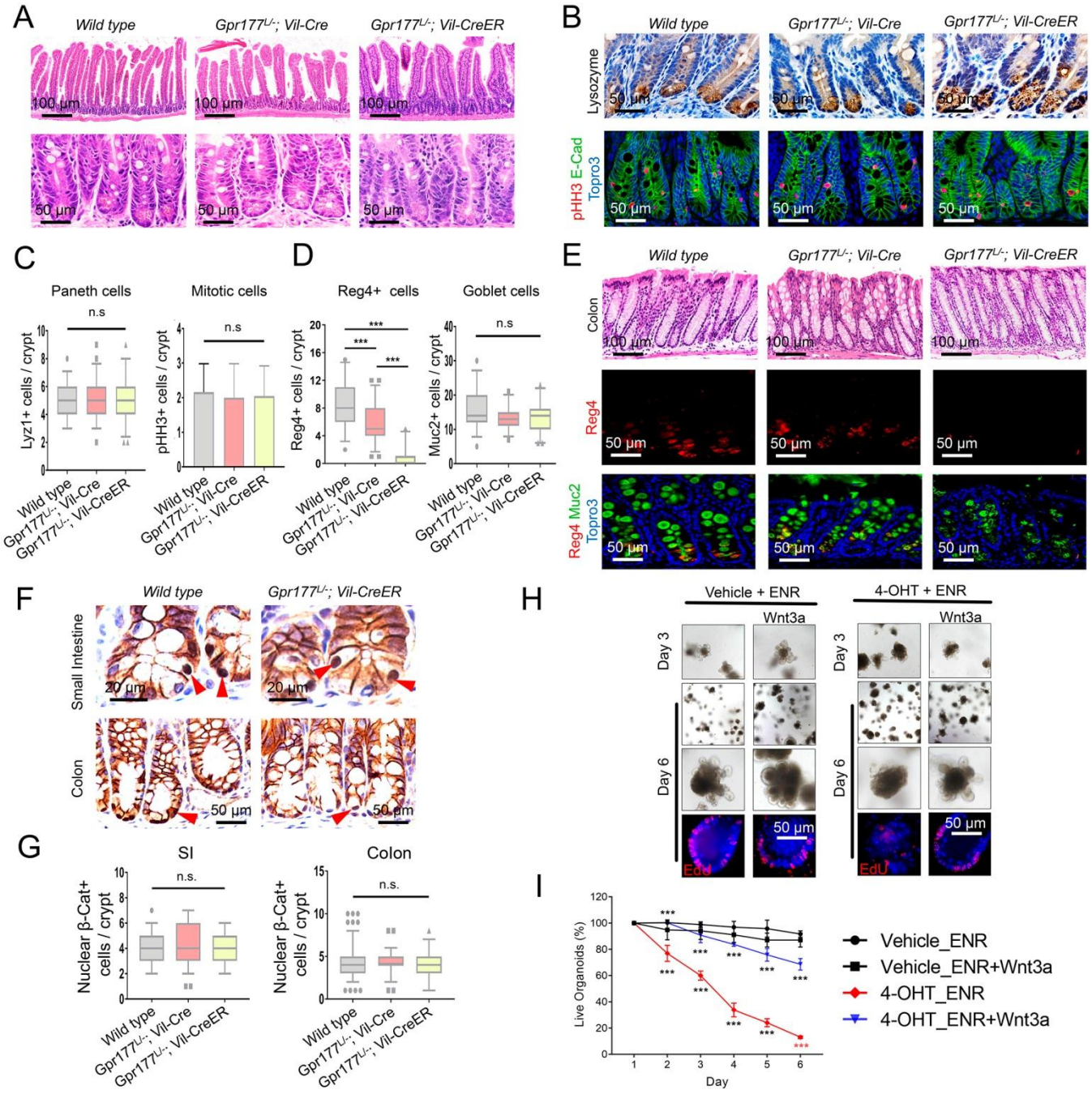

Figure 1. Blockage of epithelial Wnts impaired colonic Reg4+ cell differentiation.
(A) Histology of *Gpr177$^{L/-}$;Vil-Cre* and *Gpr177$^{L/-}$;Vil-CreER* mouse small intestines did not show difference from WT controls.
(B) Immunohistochemistry for Lysozyme and pHH3 showed normal Paneth and mitotic cells.
(C) The numbers of Paneth or mitotic cells per crypt were not changed (N=3 mice per genotype).

(D) The numbers of Reg4+ deep crypt secretory (DCS) colonic cells, but not goblet cells, were significantly decreased in *Gpr177$^{L/-}$;Vil-Cre* and *Gpr177$^{L/-}$;Vil-CreER* mouse colons (N=3 mice per genotype).
(E) Histology and Reg4/Muc2 staining showed reduced Reg4+ cells in *Gpr177$^{L/-}$;Vil-Cre* and *Gpr177$^{L/-}$;Vil-CreER* mouse colons.
(F) Immunohistochemistry for β-catenin showed unchanged nuclear β-catenin positive cells in *Gpr177$^{L/-}$;Vil-Cre* and *Gpr177$^{L/-}$;Vil-CreER* mouse small intestinal or colonic crypts.
(G) The numbers of nuclear β-catenin positive cells per crypt were not changed (N=3 mice per genotype).
(H) *Gpr177$^{L/-}$;Vil-CreER* mouse enteroids cultured in ENR medium were treated with 4-OHT to delete *Gpr177*. Bright field and fluorescent EdU images represented day 3 and 6 after 4-OHT or vehicle treatment, in the presence of exogenous Wnt3a. Wnt3a notably enhanced survival at day 6 when compared to vehicle group. Data are representative of 3 independent experiments.
(I) Numbers of viable enteroids were counted daily following 4-OHT treatment. Wnt3a notably enhanced the survival of 4-OHT treated enteroids when compared to no Wnt groups. Statistical significance provided for 4-OHT_ENR+Wnt3a vs 4-OHT_ENR and 4-OHT_ENR vs Vehicle_ENR.
** p<0.05; **p<0.01; ***p<0.001.* All graphs display mean ± SEM from at least three independent experiments. **Please also see Supplementary Figure 1.**

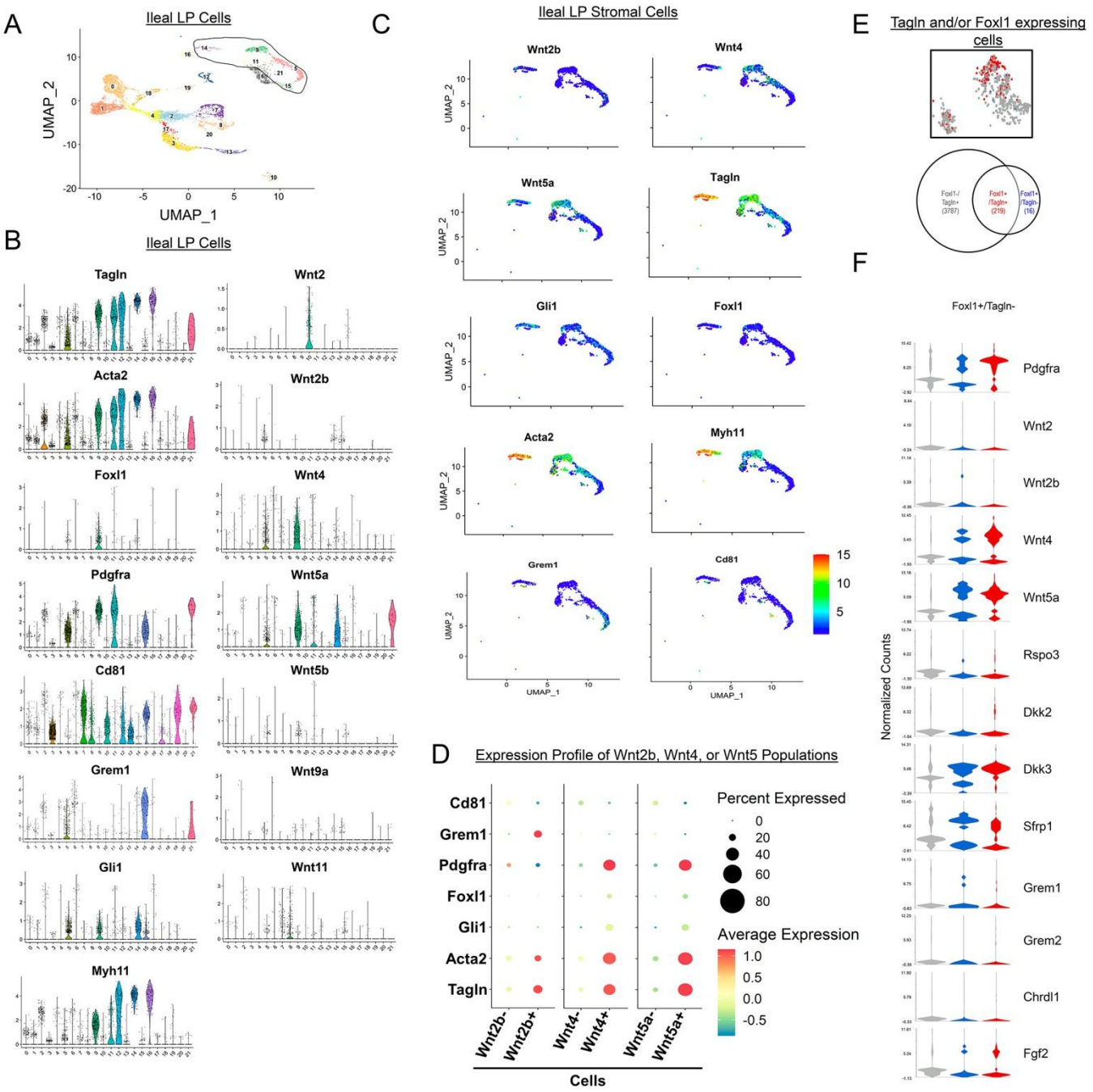

Figure 2. Tagln+ stromal domain encompassed the majority of subepithelial Wnt producers. (A) Uniform manifold approximation and projection (UMAP) of 8,767 mouse ileal stromal cells resulted in 22 distinct clusters. Wnt- expressing clusters are circled on the UMAP plot.
(B) Violin plots showed the stromal domains expressing Wnt ligands and key stromal cell markers (Foxl1, Gli1, Pdgfra, Cd81, and Grem1) across the 22 clusters. Note that Tagln and Acta2 were highly expressed in the major Wnt2b-, Wnt4-, Wnt5a-expressing clusters.
(C) UMAP plots for clusters 5, 9, 11, 14, and 21 showed a containment of these Wnt-producing cells by Tagln and Acta2.

(D) Differential expression of Tagln, Acta2, Foxl1, Gli1, Pdgfra, Grem1, and Cd81 in Wnt2b- and Wnt2b+ cell, Wnt4- and Wnt4+ cells, and Wnt5a- and Wnt5a+ cells.
(E) t-SNE plot and venn diagram highlighted Tagln+/Foxl1-, Tagln+/Foxl1+, and Tagln-/Foxl1+ populations with exact number of cells in each population. Note that 16 out of 235 Foxl1+ cells did not express Tagln.
(F) Violin plots showed a similar transcriptomic expression between Tagln+/Foxl1+ and Tagln-/Foxl1+ populations, for Wnt, R-Spondin, DKK, Fgf, Sfrp1, and Grem molecules. **Please also see Supplementary Figure 2.**

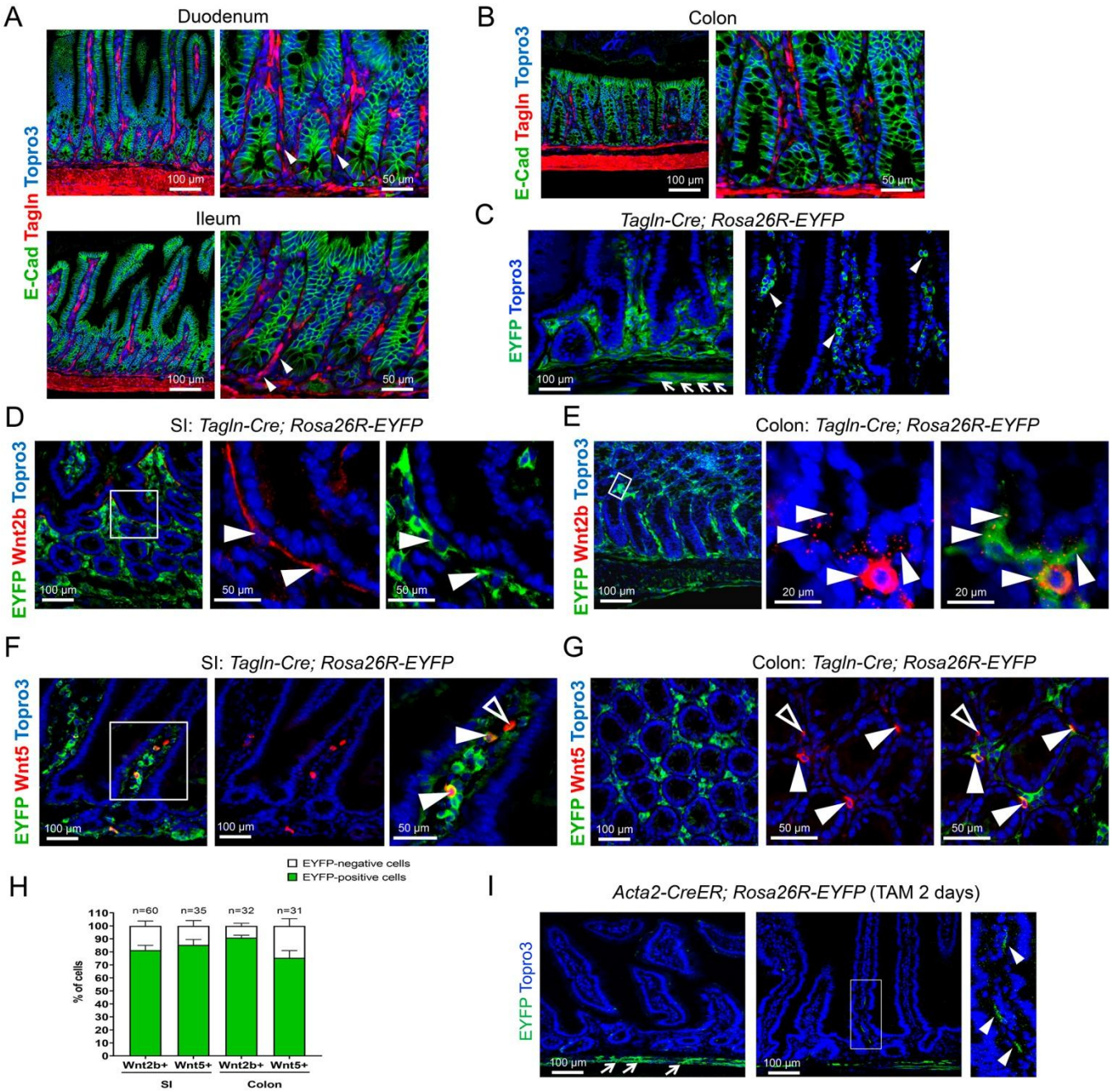

Figure 3. Tagln-Cre and Acta2-CreER targeted anatomically different stromal compartments.
(A-B) Immunostaining for Tagln (SM22) showed a broad Tagln-expressing stromal domain in small intestine and colon. Note some Tagln+ cells were in immediate proximity to crypts.
(C) *Tagln-Cre; Rosa26R-EYFP* mice showed Cre-mediated recombination in stromal domain in a similar pattern as endogenous Tagln+ cells.
(D-G) Co-staining of Wnt2b or Wnt5 with EYFP in *Tagln-Cre; Rosa26R-EYFP* mouse small intestines and colons showed Cre-activated reporter expression in Wnt2b+ and Wnt5+ cells (white arrowheads). Cells that did not show EYFP were indicated by open arrowheads.

(H) The vast majority of Wnt2b+ and Wnt5+ cells were labeled by Tagln-Cre.
(I) *Acta2-CreER; Rosa26R-EYFP* mice showed a different Cre reporter domain towards the outer smooth muscle layers of the intestine. All graphs display mean ± SEM from at least three independent experiments. **Please also see Supplementary Figure 3.**

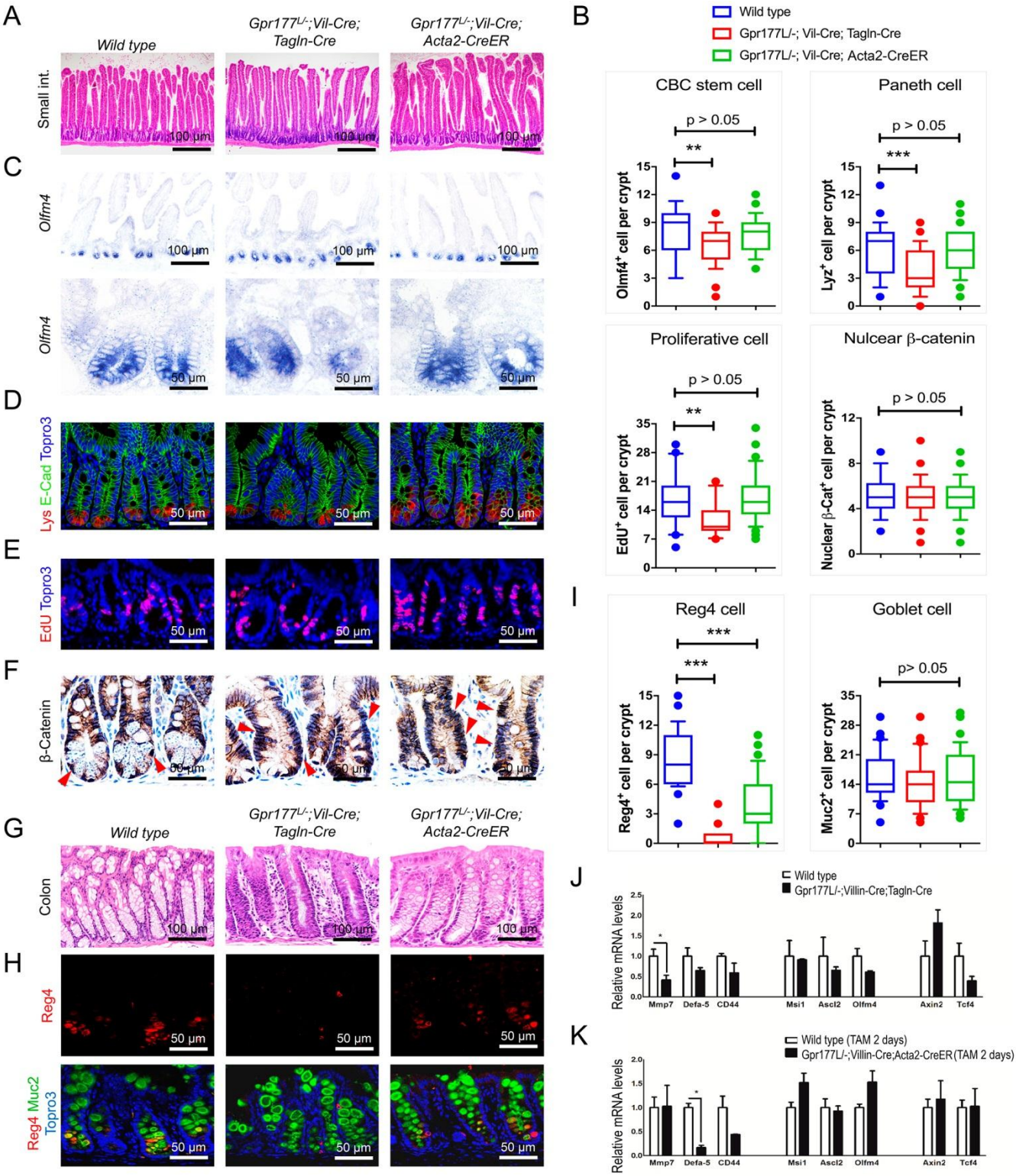

Figure 4. Wnt deprivation from epithelium and Tagln+ or Acta2+ cells diminished Reg4 cell differentiation in colon.
(A) Histology analysis did not show difference in *Gpr177$^{L/-}$;Vil-Cre;Tagln-Cre* and *Gpr177$^{L/-}$;Vil-Cre;Acta2-CreER* mouse small intestines.
(B-F) *Gpr177$^{L/-}$;Vil-Cre;Tagln-Cre* intestines had reduced Olfm4+ (C), Lyz1+ (D), EdU+ (E) cell numbers but unchanged number of nuclear β-catenin (red arrowheads) positive cells (F). *Gpr177$^{L/-}$;Vil-Cre;Acta2-CreER* mice showed no detectable difference in the above analysis. N=3 mice per genotype. 50 crypts of the small intestine were counted per marker per genotype.
(G-I) Histology and immunostaining for Reg4 and Muc2 showed diminished and significantly reduced DCS cells (H) in *Gpr177$^{L/-}$;Vil-Cre;Tagln-Cre* and *Gpr177$^{L/-}$;Vil-Cre;Acta2-CreER* mouse colons, respectively. Goblet cells were not changed. N=3 mice per genotype.
(J-K) Quantitative RT-PCR detected a reduction in *Mmp7* in *Gpr177$^{L/-}$;Vil-Cre;Tagln-Cre* intestines and a reduction in *Defa5* in *Gpr177$^{L/-}$;Vil-Cre;Acta2-CreER* intestines. N=3 mice per genotype. All graphs display mean ± SEM from at least three independent experiments. **Please also see Supplementary Figure 4.**

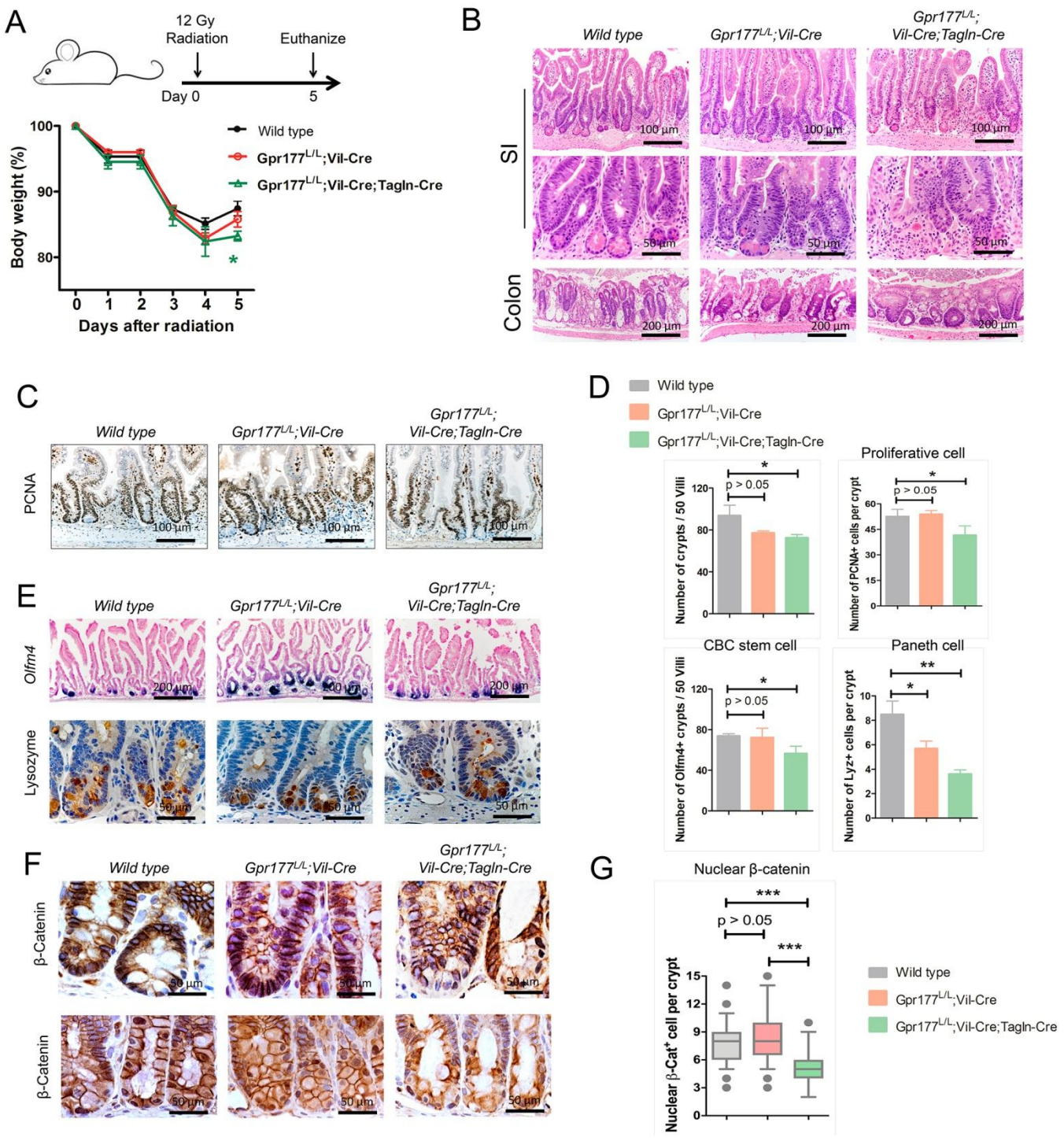

Figure 5. Blocking Wnts from epithelium and Tagln+ cells modestly affected irradiation-induced regeneration.

(A) Schematic diagram and body weight analysis of mice exposed to 12Gy total body irradiation. The *Gpr177$^{L/L}$;Vil-Cre;Tagln-Cre* mice showed a modestly significant body weight reduction at day 5 after irradiation. N=6 mice per genotype.

(B-E) Post-irradiated *Gpr177$^{L/L}$;Vil-Cre;Tagln-Cre* mice had reduced regenerative crypts (B), PCNA- positive proliferating crypt cells (C), Olfm4+ cells in the crypt (E), and Lyz1+ cells in the crypt (E). *Gpr177$^{L/L}$;Vil-Cre* mice showed modestly reduced Lyz1+ cells. (D) Number of crypts, PCNA+ cells, Olfm4+ crypts, and Lyz1+ cells were quantified for wild type, *Gpr177$^{L/L}$;Vil-Cre,* and *Gpr177$^{L/L}$;Vil-Cre;Tagln-Cre mice* intestines shown by representative images. N=3 mice per genotype.

(F-G) *Gpr177$^{L/L}$;Vil-Cre;Acta2-CreER* mice showed reduced number of nuclear β-catenin positive cells in regenerating crypts of distinct small intestinal regions (N=3 mice per genotype).

All graphs display mean ± SEM from at least three independent experiments.

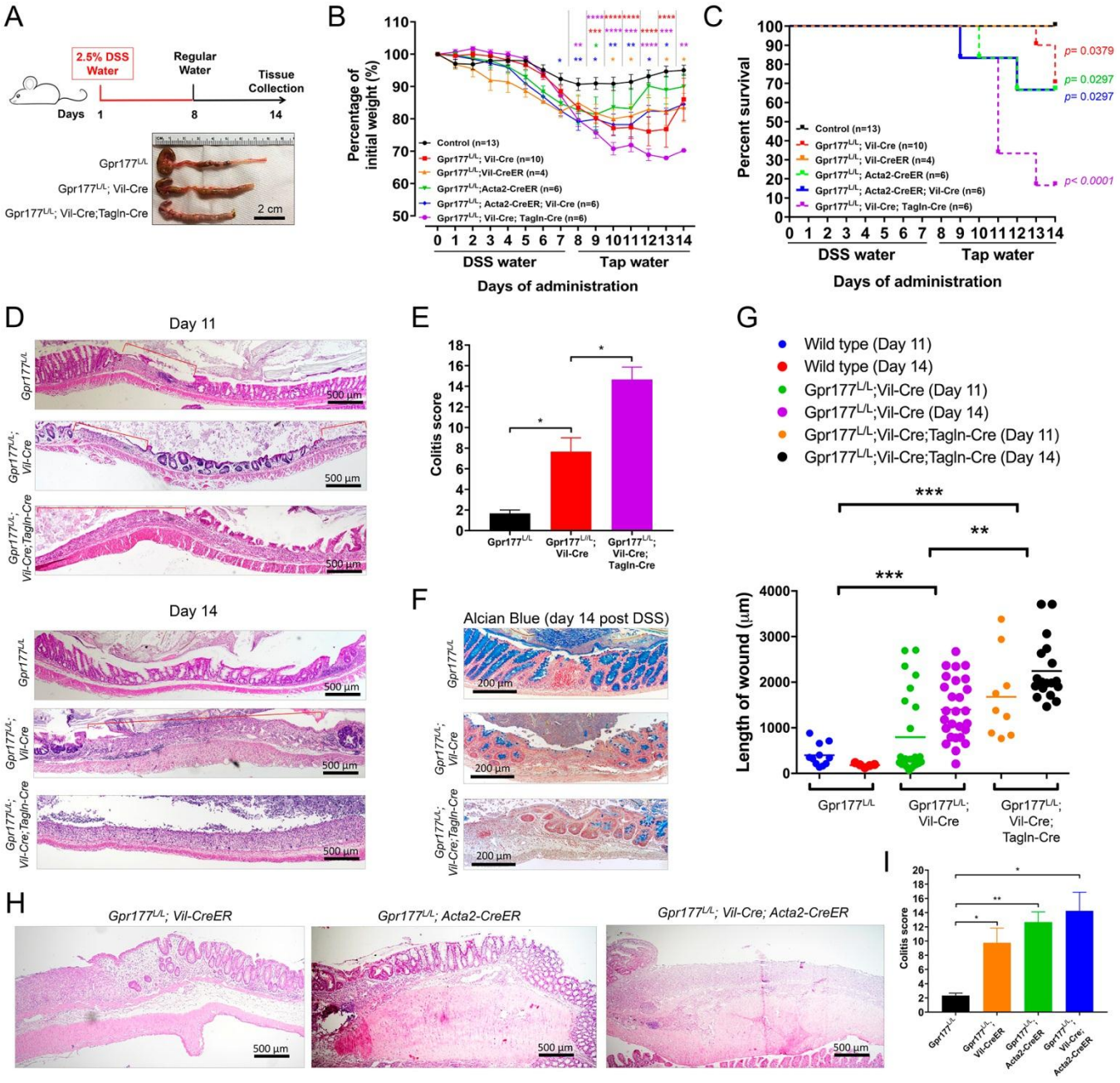

Figure 6. Colonic regeneration required Wnts from epithelial and distinct stromal compartments.

(A) Experimental scheme showing 7 days of 2.5 % DSS treatment and 7 days of recovery by administering regular drinking water. Representative colon photographs at the end of the experiment (day 14) showed a reduced colon length and small cecum of *Gpr177$^{L/L}$;Vil-Cre;Tagln-Cre* mice.

(B) Body weight analysis of mice of various genotypes, with indicated numbers, showed increased morbidity when either epithelial or stromal Wnts were blocked. Note that *Gpr177$^{L/L}$;Vil-Cre;Tagln-Cre* mice (purple line) exhibited the worst disease activities with

minimal body weight recovery. “Controls” included Gpr177 flox/flox (no cre) littermates, as well as Vil-Cre only mice, and tamoxifen-injected WT and Vil-CreER mice (non-littermates). Please also see Supplementary Figure 5A.

(C) No mortality was observed for WT mice during the experiment, while increased lethality was found for *Gpr177$^{L/L}$;Vil-Cre;Tagln-Cre* (purple line) and *Gpr177$^{L/L}$;Vil-Cre;Acta2-CreER* mice (blue line). “Controls” included Gpr177 flox/flox (no cre) littermates, as well as Vil-Cre only mice, and tamoxifen-injected WT and Vil-CreER mice (non-littermates). Please also see Supplementary Figure 5A.

(D) Representative colon histology images of day 11 and day 14 mice following DSS treatment. Red brackets indicated regions of epithelial ulceration.

(E) Scoring of mucosal damages showed increased disease indexes in *Gpr177$^{L/L}$;Vil-Cre* and *Gpr177$^{L/L}$;Vil-Cre;Tagln-Cre* mice.

(F) Alcian blue staining showed a reduction of goblet cell differentiation in recovering colons of *Gpr177$^{L/L}$;Vil-Cre* and *Gpr177$^{L/L}$;Vil-Cre;Tagln-Cre* mice.

(G) Microscopic measurement of the lengths of ulceration, at day 11 and 14, showed an advancement of the pathologies in *Gpr177$^{L/L}$;Vil-Cre* and *Gpr177$^{L/L}$;Vil-Cre;Tagln-Cre* mice. Note that *Gpr177$^{L/L}$;Vil-Cre;Tagln-Cre* colons had the largest epithelial wounds.

(H-I) Histology and colitis-scoring of mouse colons at day 14 of experiments showed worse colitis in *Gpr177$^{L/L}$;Acta2-CreER* and *Gpr177$^{L/L}$;Vil-CreER* mice while the worst disease index in *Gpr177$^{L/L}$;Vil-Cre;Acta2-CreER* mice. All graphs display mean ± SEM from at least three independent experiments. **Please also see Supplementary Figure 5.**

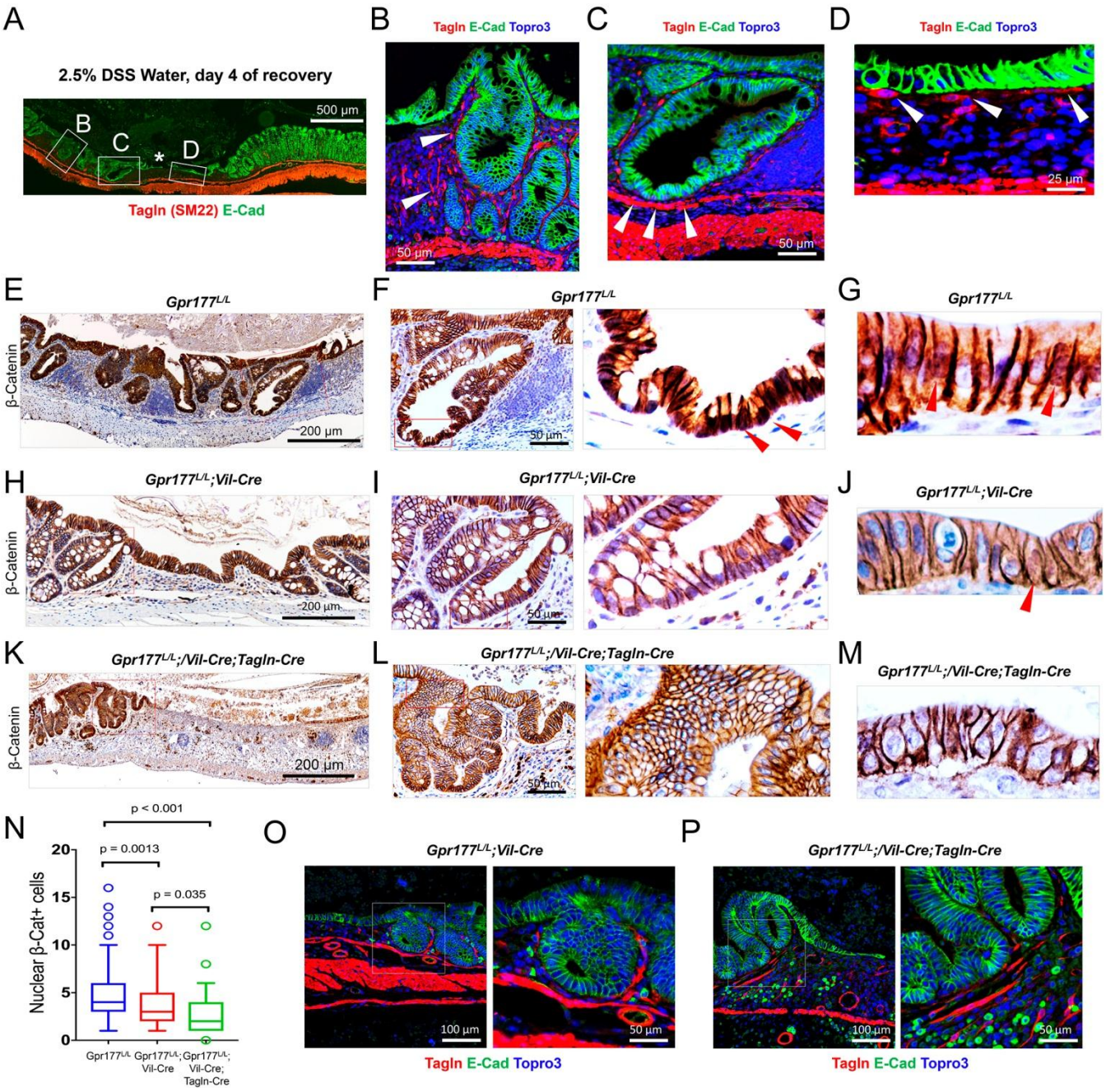

Figure 7. Tagln+ cells promoted β-catenin nuclear localization in regenerative colon epithelial cells.

(A-D) Immunostaining for endogenous Tagln+ cells showed their adjacent localizations to regenerative crypt (B), at base of wound-flanking nascent crypt (C), and underneath of wound-covering epithelial monolayer (D). Asterisk denoted an ulcerated region flanked by regenerating epithelia.

(E-N) Immunostaining showed strong nuclear β-catenin (red arrows) in WT regenerating colonic epithelium within crypt cells (F) and within wound-covering epithelial cells (G). Reduced

numbers of nuclear β-catenin cells were found in wound-flanking epithelium of *Gpr177$^{L/L}$;Vil-Cre* (H-J) and *Gpr177$^{L/L}$;Vil-Cre;Tagln-Cre* (K-M) mouse colons.
(O-P) Immunostaining showed the presence of Tagln+ cells near the regenerative crypts of *Gpr177$^{L/L}$;Vil-Cre* and *Gpr177$^{L/L}$;Vil-Cre;Tagln-Cre* mouse colons, suggesting the diminished epithelial nuclear β-catenin and regeneration were due to lack of Wnt productions rather than lack of Tagln+ cells. All graphs display mean ± SEM from at least three independent experiments. **Please also see Supplementary Figure 6.**

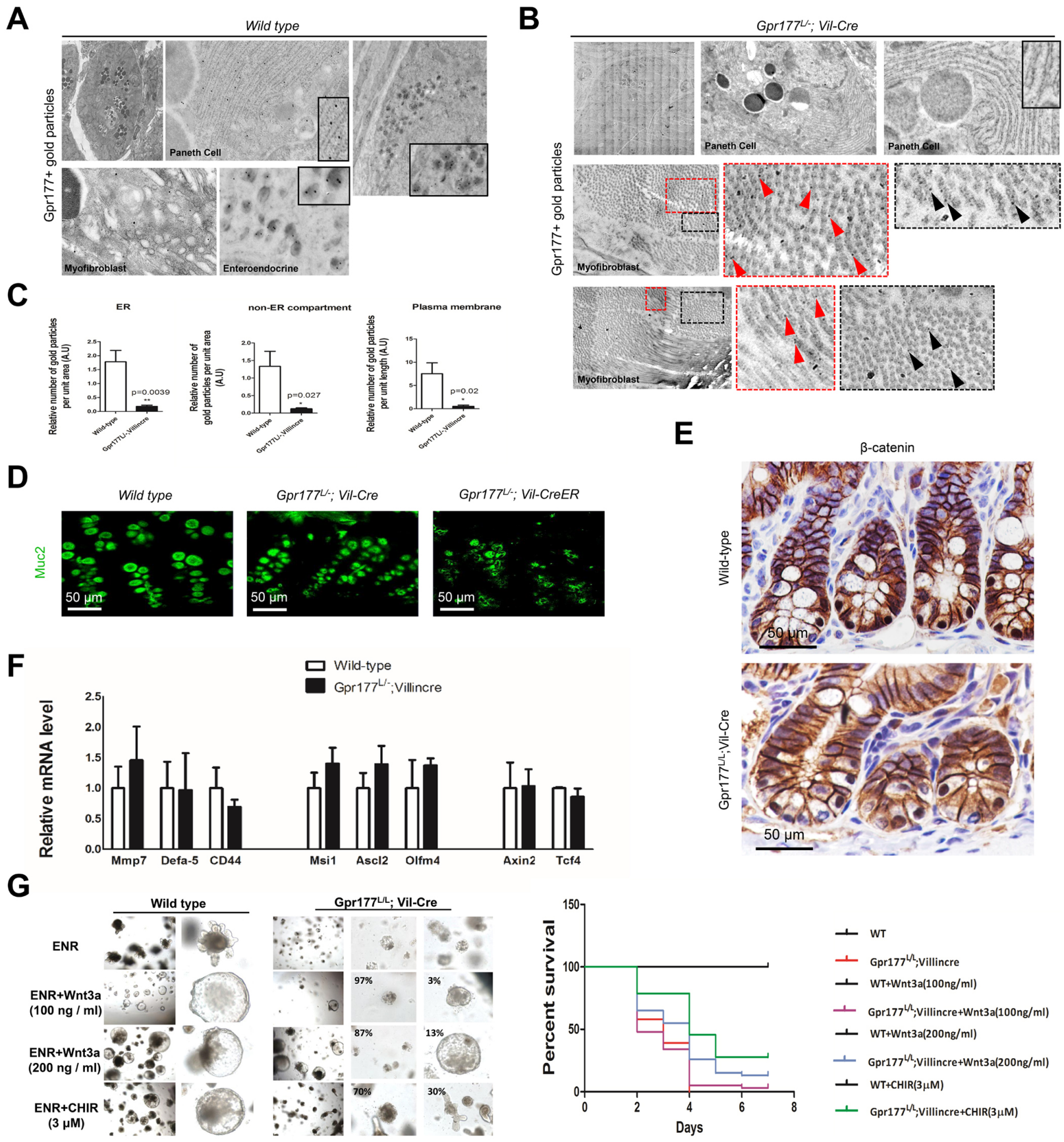

Fig. S1. (A) Transmission electron microscopy (TEM) revealed presence of Gpr177+ immunogold particles in intestinal epithelial cells, specifically Paneth cells and enteroendocrine cells, and myofibroblasts in wild type intestines. (B) TEM showed reduction in the number of Gpr177+ immunogold particles in the Paneth cells of *Gpr177$^{L/-}$;Vil-Cre* intestines while there was no change in the immunogold particle numbers in the stromal cells (red and black arrowheads). (C) Number of Gpr177+ colloidal gold particles quantified in ER, non-ER (Golgi/vesicle) and plasma membrane along with the area (ER and non-ER) or perimeter (plasma membrane) covered by each compartment in wild-type and *Gpr177$^{L/-}$; Vil-Cre* Paneth cells.
(D) Muc2 staining of wild type, *Gpr177$^{L/-}$;Vil-Cre*, and *Gpr177$^{L/-}$;Vil-CreER* mouse colons.
(E) Immunostaining showed that number of nuclear β-catenin positive cells was not changed between wild type and *Gpr177$^{L/L}$;Vil-Cre* mouse small intestinal crypts.
(F) Quantitative RT-PCR showed no change in ISC (Msi1, Ascl2, Olfm4, Axin2, and Tcf4)and Paneth cell (Mmp7, Defa-5, and CD44) signature genes in *Gpr177$^{L/-}$;Vil-Cre* mouse intestines. N=3 for each genotype.
(G) Enteroids were grown from ileal crypts of wild type and *Gpr177$^{L/L}$;Vil-Cre* mice, cultured in ENR or ENR supplemented with Wnt3a (100 ng/ml or 200 ng/ml) or CHIR (3 µM). *Gpr177$^{L/L}$;Vil-Cre* mouse enteroids failed to grow in ENR medium. The bolded percentage for *Gpr177$^{L/L}$;Vil-Cre* mouse enteroids indicates the population of organoids similar to the representative image. Exogenous Wnt3a (200 ng/mL, blue line) and CHIR (green line) enhanced survival of a fraction of Gpr177$^{L/-}$;Vil-Cre mouse enteroids.

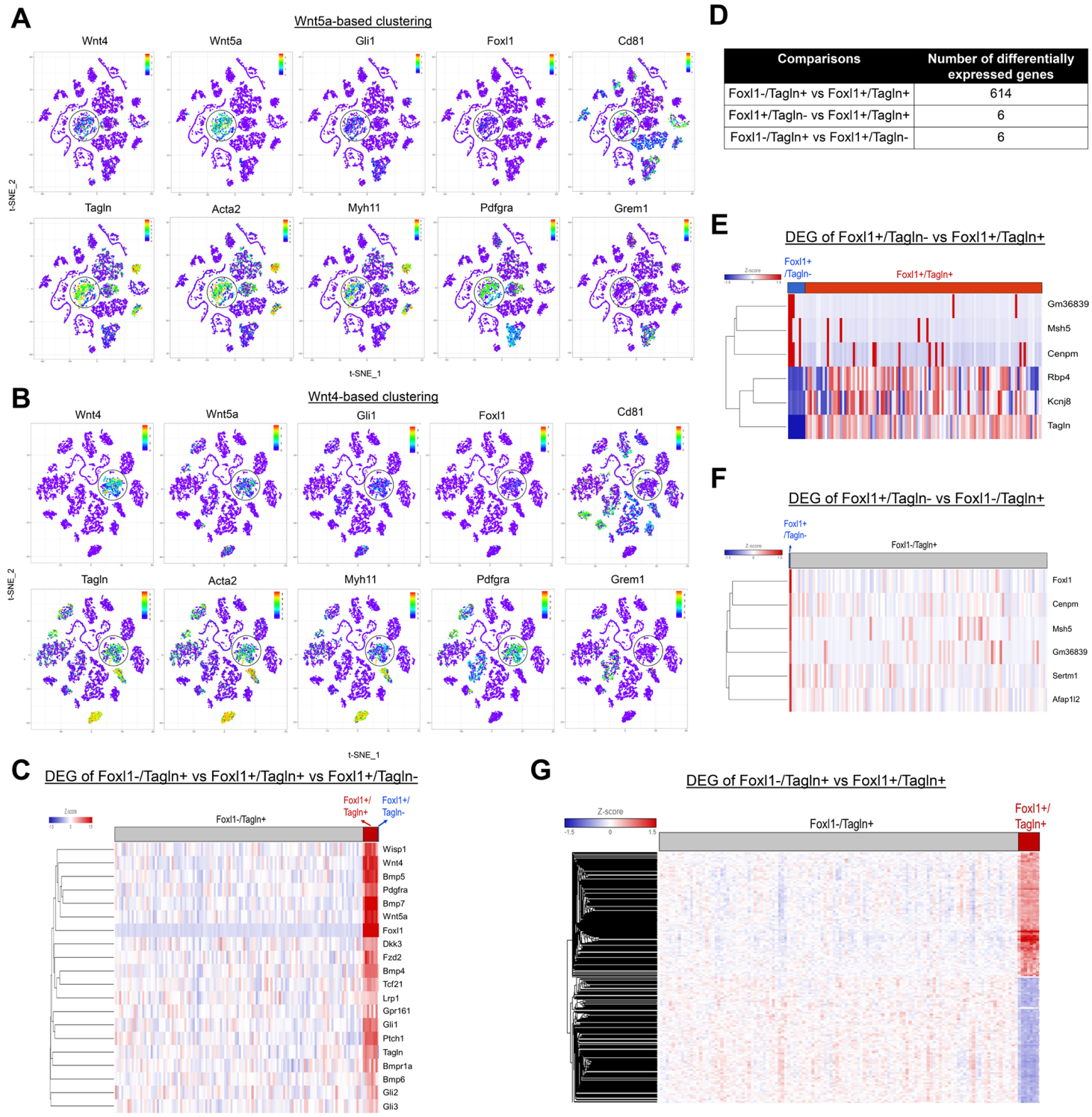

Fig. S2. (A) t-SNE plot of Wnt5a-based Single Cell Deep Constrained Clustering (scDCC) of the mouse ileal stromal cells. Wnt5a-expressing cells (circled in black) highly co-expressed Wnt4, Tagln, Acta2, Pdgfra, and Myh11.

(B) t-SNE plot of Wnt4-based scDCC clustering of the mouse ileal stromal cells. Wnt4-expressing cells (circled in black) highly co-expressed Wnt5a, Tagln, Acta2, Pdgfra, and Myh11.

(C) Heatmap of the transcriptomes of Tagln+/Foxl1-, Tagln+/Foxl1+, and Tagln-/Foxl1+ populations indicated a Foxl1-driven expression change in Tagln+/Foxl1+ cells.

(D) Table summarizing the number of differentially expressed genes between Foxl1-/Tagln+ and Foxl1 +/Tagln+, Foxl1+/Tagln- and Foxl1+/Tagln+, Foxl1-/Tagln+ and Foxl1+/Tagln- populations. (E) Heatmap showed relative expression of the 6 genes differentially expressed between Foxl1+ /Tagln- and Foxl1+/ Tagln+ populations.

(F) Heatmap showed the relative expression of the 6 genes differentially expressed between Foxl1-/ Tagln+ and Foxl1+/Tagln- populations.

(G) Heatmap showed relative expression of the 614 differentially expressed genes detected between Foxl1-/Tagln+ and Foxl1+/Tagln+ populations.

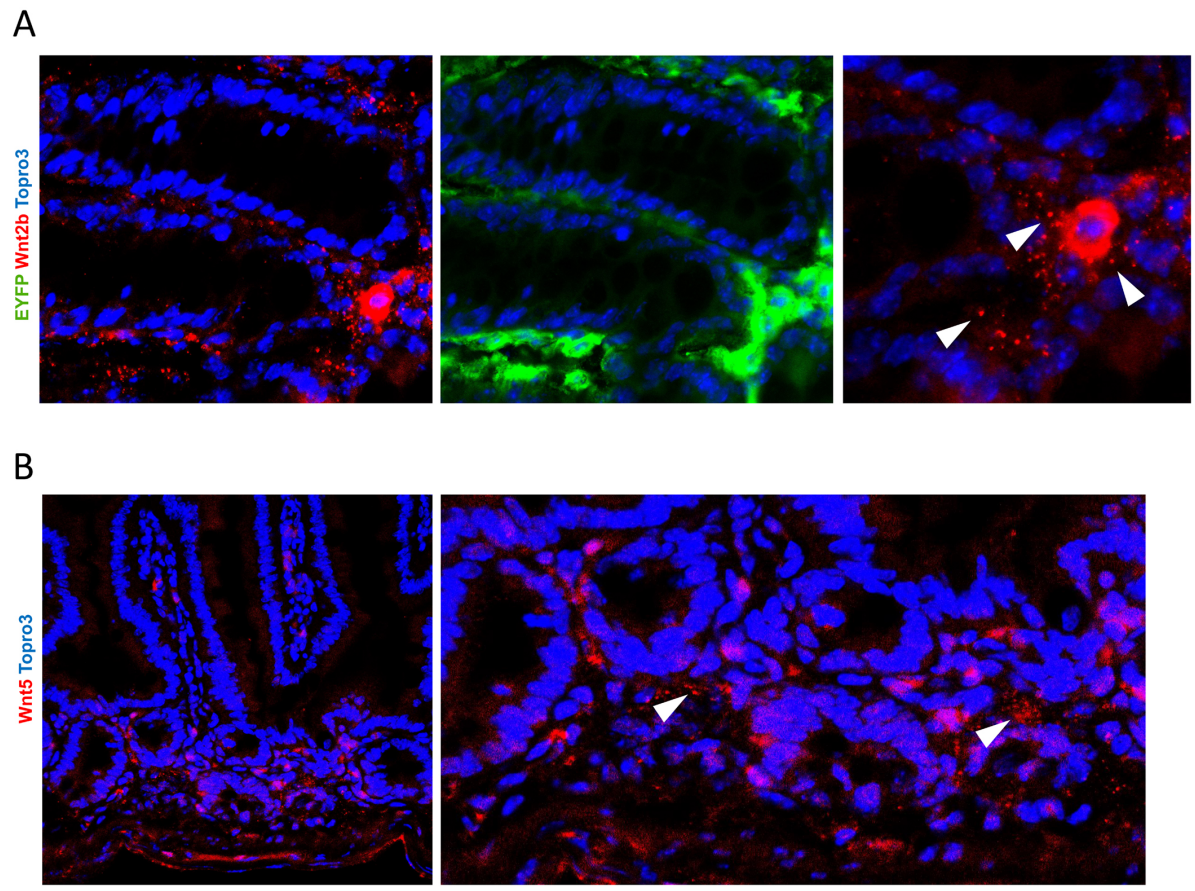

Fig. S3. (A) Co-staining of Wnt2b with EYFP in *Tagln-Cre; Rosa26R-EYFP* mouse colons showed Cre-activated reporter expression in Wnt2b+ cells (white arrowheads).
(B) Staining of Wnt5 in *Tagln-Cre; Rosa26R-EYFP* mouse small intestines revealed perinuclear and vesicular localization of Wnt5 (white arrowheads).

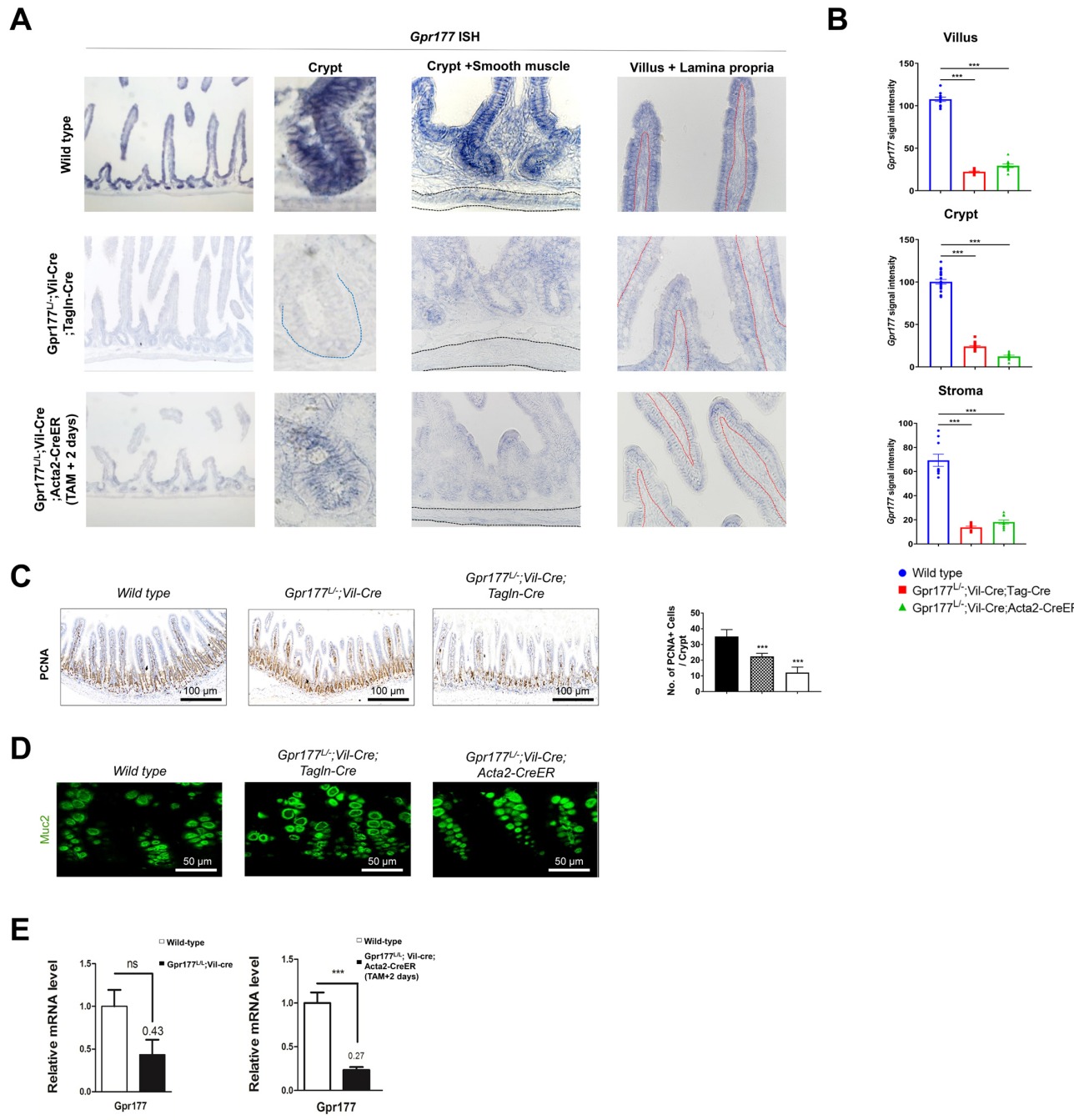

Fig. S4. (A-B) RNA *in situ* hybridization of Gpr177 revealed significant deletion in villus, crypt, and stromal cells of *Gpr177$^{L/-}$;Vil-Cre;Tagln-Cre* and *Gpr177$^{L/L}$;Vil-Cre;Acta2-CreER* mice. The blue dotted line delineates the crypt, black dotted lines delineate smooth muscles, and red dotted lines delineate the lamina propria.
(C) Immunohistochemistry of PCNA showed reduction in numbers of proliferating cells in *Gpr177$^{L/L}$;Vil-Cre* and *Gpr177$^{L/-}$;Vil-Cre;Tagln-Cre* mice.
(D) The number of Muc2+ cells were unchanged between wild type, *Gpr177$^{L/-}$;Vil-Cre;Tagln-Cre* and *Gpr177$^{L/-}$;Vil-Cre;Acta2-CreER* mouse colons.
(E) RT-PCR of Gpr177 showed no change between wild type and *Gpr177$^{L/L}$;Vil-Cre* intestines while there was a significant reduction in *Gpr177$^{L/L}$;Vil-Cre;Acta2-CreER* intestines compared to wild type

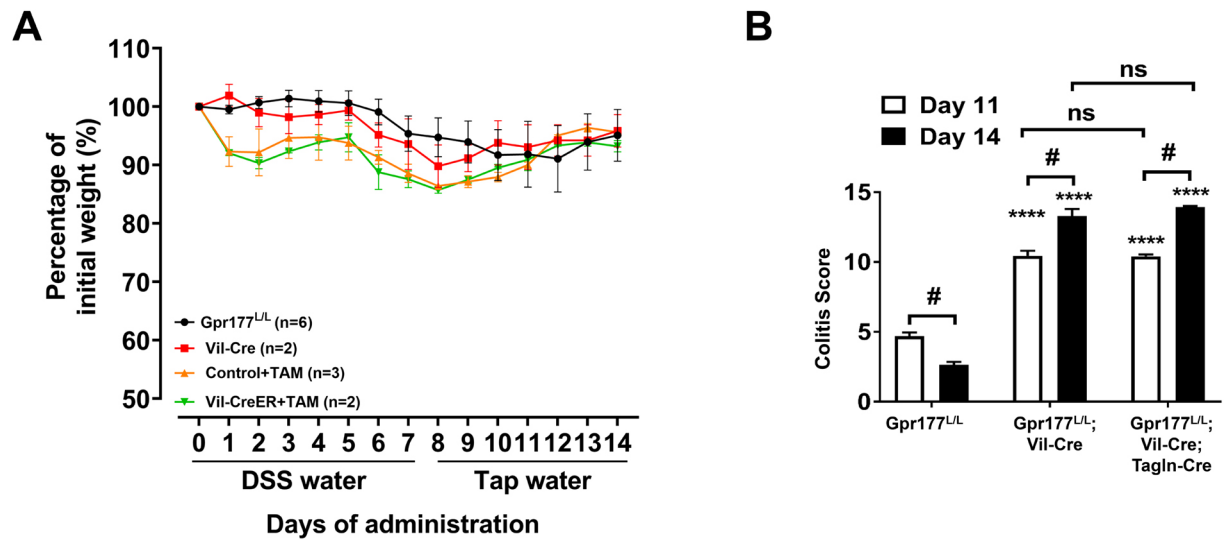

Fig. S5. (A) Body weight analysis of control mice included Gpr177 flox/flox (no cre) littermates, as well as Vil-Cre only mice, and tamoxifen-injected WT and Vil-CreER mice (non-littermates), with indicated numbers, did not show any significant difference.
(B) Colitis scored by a different matrix consisting of ulceration, crypt death, immune cell infiltration, thickness of colonic wall, and loss of goblet cell showed increased pathological indexes in *Gpr177$^{L/L}$;Vil-Cre* and *Gpr177$^{L/L}$;Vil-Cre;Tagln-Cre* mice.

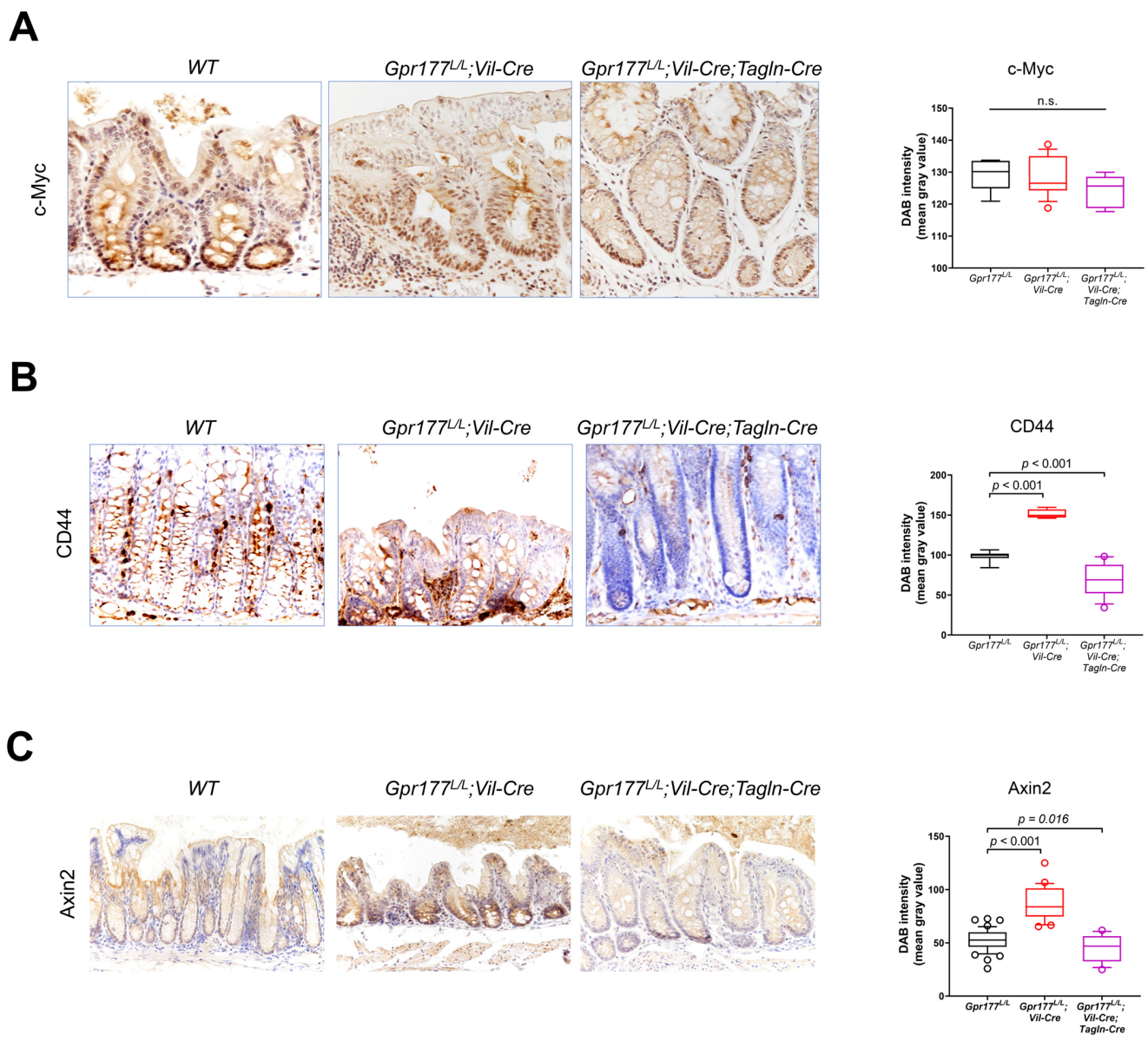

Fig. S6. (A) Immunohistochemistry and quantification of c-Myc in DSS-treated *Gpr177$^{L/L}$*, *Gpr177$^{L/L}$;Vil-Cre,* and *Gpr177$^{L/-}$;Vil-Cre;Tagln-Cre* mouse colons.

(B) Immunohistochemistry and quantification of CD44 in DSS-treated *Gpr177$^{L/L}$*, *Gpr177$^{L/L}$;Vil-Cre,* and *Gpr177$^{L/-}$;Vil-Cre;Tagln-Cre* mouse colons.
(C) Immunohistochemistry and quantification of Axin2 in DSS-treated *Gpr177$^{L/L}$*, *Gpr177$^{L/L}$;Vil-Cre,* and *Gpr177$^{L/-}$;Vil-Cre;Tagln-Cre* mouse colons.
Significance of differences was determined by two-tailed t test.

Table S1. Sequences of the quantitative RT-PCR primers

Gene	Forward	Reverse
Tcf4	AGCCCGTCCAGGAACTATG	TGGAATTGACAAAAGGTGGA
Axin2	TGAGATCCACGGAAACAGC	GTGGCTGGTGCAAAGACAT
Gpr177	CAAATCGTTGCCTTTCTGGT	CGCCAGCCATCTTGTTTTAT
Mmp7	CTTACAAAGGACGACATTGCAG	AGTGCAGACCGTTTCTGTGAT
Defa5	TATCTCCTTTGGAGGCCAAG	TTTCTGCAGGTCCCAAAAAC
CD44	CACCATTGCCTCAACTGTGC	TTGTGGGCTCCTGAGTCTGA
Ascl2	TCCAGTTGGTTAGGGGGCTA	GCATAGGCCCAGGTTTCTTG
Olfm4	GCCACTTTCCAATTTCAC	GAGCCTCTTCTCATACAC
β-actin	TTGCTGACAGGATGCAGAAG	CCACCGATCCACACAGAGTA
Hprt	AAGCTTGCTGGTGAAAAGGA	TTGCGCTCATCTTAGGCTTT